Immunology and Inflammation

Diversity and functional specialization of oyster immune cells uncovered by integrative single cell level investigations

Sébastien de La Forest Divonne, Juliette Pouzadoux, Océane Romatif, Caroline Montagnani, Guillaume Mitta, Delphine Destoumieux-Garzon, Benjamin Gourbal, Guillaume M Charrière, Emmanuel Vignal

IHPE, Univ Montpellier, CNRS, Ifremer, Univ Perpignan Via Domitia, Montpellier, France • Ifremer, IRD, Institut Louis-Malardé, Univ Polynésie française, UMR 241 SECOPOL, Taravao, Tahiti - Polynésie française, France • IHPE, Univ Montpellier, CNRS, Ifremer, Univ Perpignan Via Domitia, Perpignan, France

Reviewed Preprint
v3 • April 11, 2025
Revised by authors

Reviewed Preprint
v2 • March 25, 2025

Reviewed Preprint
v1 • November 13, 2024

eLife Assessment

The manuscript by de La Forest Divonne et al. offers an **important** and detailed exploration of the immune cells in the oyster Crassostrea gigas, by correlating distinct hemocyte morphotypes with specific single-cell transcriptional profiles. The evidence supporting the conclusion is **convincing**, deriving from the comprehensive dataset that not only captures unicellular diversity but also associates these cells with distinct immune roles, making it an invaluable resource for the broader research community.

https://doi.org/10.7554/eLife.102622.3.sa2

Abstract

Mollusks are a major component of animal biodiversity and play a critical role in ecosystems and global food security. The Pacific oyster, *Crassostrea (Magallana) gigas*, is the most farmed bivalve mollusk in the world and is becoming a model species for invertebrate biology. Despite the extensive research on hemocytes, the immune cells of bivalves, their characterization remains elusive. Here we were able to extensively characterize the diverse hemocytes and identified at least seven functionally distinct cell types and three hematopoietic lineages. A combination of single-cell RNA sequencing, quantitative cytology, cell sorting, functional assays and pseudo-time analyses was used to deliver a comprehensive view of the distinct hemocyte types. This integrative analysis enabled us to reconcile molecular and cellular data and identify distinct cell types performing specialized immune functions, such as phagocytosis, reactive oxygen species production, copper accumulation, and expression of antimicrobial peptides. This study emphasized the need for more in depth studies of cellular immunity in mollusks and non-model invertebrates and set the ground for further comparative immunology studies at the cellular level.

Introduction

Mollusca is the second largest invertebrate phylum, after Arthropoda, and the largest marine phylum, comprising approximately 23 % of all known marine organisms (1). Among them, bivalves exhibit a high diversity and a rich evolutionary history (2). The Pacific oyster *Crassostrea (Magallana) gigas* (*C. gigas* - Thunberg, 1793) (NCBI:txid29159) is a sessile filter-feeding bivalve that thrives in a variety of stressful environments ranging from intertidal to deep-sea conditions (3). It is a key species for the aquaculture industry worldwide (4). Several infectious diseases affect *C. gigas* at different life stages, which impacts its production. Given the significant socio-economic value of this species, there has been an increased focus on understanding and mitigating these diseases (5). The causes of these mortalities can involve a variety of pathogens, including viruses, bacteria and parasites that can be responsible for the mortality events affecting *C. gigas* (6). One of the most extensively researched infectious diseases is POMS (Pacific Oyster Mortality Syndrome), a polymicrobial disease responsible for mass mortalities of juvenile oysters (7). The disease is triggered by the OsHV-1 µVar herpesvirus, which alters the immune defenses of oysters, allowing the colonization of opportunistic bacteria, including *Vibrio*, that cause hemocyte lysis and bacteremia, ultimately leading to animal death (7). Other bacterial pathogens have also been identified as a contributing factor in mass mortalities of adult Pacific oysters in several countries. The most notable is *Vibrio aestuarianus* which affects adult oysters in Europe (8, 9). To date, the majority of oyster pathogens or opportunistic pathogens that have been characterized in detail have been found to subvert hemocyte defenses for their own benefit. These include the OsHV-1 µVar herpesvirus (10) and virulent *Vibrio* strains of the species *Vibrio crassostreae* and *Vibrio tasmaniensis* (11), *Vibrio aestuarianus* and *Vibrio harveyi* (12), highlighting the critical role of hemocytes in oyster immunity. The development of immune-based prophylactic treatments, such as immune-priming and immune-shaping, represents a promising avenue for enhancing the natural defenses of oysters against pathogens and increasing their survival rate. Nevertheless, the advancement of such therapies is still constrained by a dearth of knowledge regarding the underlying molecular and cellular mechanisms (13, 14).

The study of hemocytes has a long history, dating back to the 1970s (for review see (15)). Hemocytes are cellular effectors of the immune system. They engage in phagocytosis to engulf and destroy potential pathogens, neutralizing parasites by encapsulation, or preventing pathogen dissemination by cell aggregation and the release of extracellular DNA traps (16). Furthermore, they engage in the humoral response by releasing cytokines, antimicrobial peptides, and reactive oxygen species (ROS), which enable them to combat pathogens (17). In addition to their role in oyster immunity, hemocytes have been implicated in numerous physiological processes, including shell repair (18), wound healing, nutrient transport, and environmental contaminant removal (19). Despite this acquired knowledge, hemocytes remain an under-characterized population of circulating immune cells. The lack of a unified classification and of molecular and functional genetic tools hinders our understanding of lineage ontogeny and functional specialization. Several studies have proposed different classifications of hemocytes in the *Ostreidae* family, with 3 to 4 hemocyte types reported (15). These classifications are primarily based on either microscopic or flow cytometry analyses. In *C. gigas*, three primary hemocyte cell types have been classically identified : blast, hyalinocyte, and granulocyte cells. Blast-like cells are considered as undifferentiated hemocyte types (20), hyalinocytes (21) seem to be more involved in wound repair, and granulocytes, more implicated in immune surveillance. The latter are considered as the main immunocompetent hemocyte types (22). While the immune response of *C. gigas* has been extensively studied using classical transcriptomics (23–25) at the whole animal, tissue, or circulating hemocyte levels, these approaches have failed to consider the diversity of hemocyte cell types and lineages that underpin these responses (26). However, it is still imperative to accurately describe the diversity of these cells, understand their ontogeny, and delineate cell

lineages to comprehend their specific roles. The advent of single-cell RNA sequencing (scRNA-seq) techniques has enabled the monitoring of global gene expression at the single-cell level with thousands of individual cells in a single experiment. This provides a unique opportunity to overcome these limitations and deepen our understanding of hemocyte diversity and function in bivalves. Recently scRNA-seq was used to provide a first molecular description of a hemocyte population in the oyster *Crassostrea hongkongensis* (27). However, in the absence of morphological and/or functional characterization studies, the authors could not deduce the hemocyte cell types to be matched to the transcriptomic profiles generated by scRNA-seq.

While numerous transcriptomic analyses have been conducted on *C. gigas* hemocytes, none have adopted a single-cell approach. In this study, we present an integrative analysis of the diversity of *C. gigas* hemocytes at the single-cell level. To this end, we combined scRNA-seq from a pathogen-free adult oyster combined with cytological, cell fractionation and functional assays. This approach allowed us to create a comprehensive transcriptomic, cytological and functional atlas of hemocyte cell types. Our scRNA-seq analyses identified 7 distinct transcriptomic populations and functional annotation revealed distinct populations with specific functions, including phagocytosis, oxidative burst, energetic metabolism, enhanced transcription, translation and cell division. Quantitative cytology enabled the identification of 7 morphologically distinct hemocyte cell types, which allowed us to reconcile molecular and cytological data. Density gradients were used to separate hemocyte cell types and qPCR or functional assay analyses were performed to validate cell type-specific markers. By employing this integrated approach, we could identify 1 type of hyalinocyte, 2 types of blasts and 4 types of granular cells. Furthermore, we identified cell types that perform antimicrobial functions through phagocytosis, ROS production, copper accumulation, and expression of antimicrobial peptides. Finally, trajectory analysis of scRNA-seq data combined with functional analysis revealed distinct differentiation pathways that may control hemocyte ontology and differentiation processes. Based on these findings, we propose a more comprehensive and up-to-date classification of *C. gigas* hemocytes, with a more accurate description of the different cell types, their potential ontology and a precise description of their sub-functionalization.

Results

Single-cell RNA sequencing reveals 7 distinct transcriptomic clusters of circulating immune cells in oysters

Oysters are known to exhibit a high degree of individual genetic polymorphism, including Copy Number Variation (CNV) and Presence Absence Variation (PAV) (28). To prevent misinterpretation of the single-cell transcriptomic data, and to characterize the hemocyte cell types and their heterogeneity, we sampled hemocytes from a unique known pathogen-free animal (Ifremer Standardized Animal, 18-month-old) and applied single-cell drop-seq technology. A total of 4,950 cells were loaded, with a target recovery of 3,000 single hemocytes for analysis. (**Fig. 1A**). The scRNA-seq library was generated and sequenced, resulting in 127,959,215 high-quality filtered reads available for single-cell analysis (ENA project accession number PRJEB74031). Primary bioinformatics analysis was performed using the STAR solo aligner software (29) against the *C. gigas* genome (Genbank reference GCA_902806645.1) from the Roslin Institute (30). Of the 127,959,215 reads, 97 % showed a valid barcode and 89.2 % were successfully mapped to the genome with a saturation of 75.6 %. A total of 2,937 cells were profiled, yielding a median of 1,578 genes and 4,412 unique molecular identifiers (UMIs) per cell among the 23,841 total genes detected, with a sequencing saturation of 75.6 % (Supp. Table S1). Secondary bioinformatic data processing was conducted using the Seurat R package (version 4.3.0) (31). The data set was filtered to remove data corresponding to empty droplets or cell doublets. Cells with a gene number between 750 and 4,000 and less than 5 % mitochondrial genes were retained. After quality control processing, 120 cells corresponding to empty droplets and cell doublets were

removed, and 2,817 cells were processed for data normalization. Finally, we performed linear dimensional reduction and clustering on the 3,000 most variable genes from 2,817 cells (Supp. Fig. S1). Dimension reduction and clustering led to identifying 7 transcriptomic clusters, within which hemocytes were distributed. These 7 different clusters represented 27.6, 23.1, 17.8, 16.9, 7, 4.6 and 3 % of the total cells (**Fig. 1B**). For each transcriptomic cluster, the heatmap displays the top 10 positively enriched marker genes identified by Seurat's differential expression analysis, highlighting cluster-specific overexpression (**Fig. 1C**).

Average Log2FC values and percentage of expression in each cluster relative to all other clusters were calculated for the ten most differentially expressed genes (**Fig. 1D** and **Table 1**). Clear transcriptomic cell clusters were detected as well as specific gene markers for each cluster (**Supp. Data 1**). Only the transcriptomic signature of cluster 4 was less contrasting than that of the other clusters (**Fig. 1D**).

KEGG pathways and GO-terms analyses reveal functional diversity in *C. gigas* hemocytes

The ScRNA-seq data demonstrated that specific functions are carried out by the hemocyte cell types that comprise the seven transcriptomic clusters. A preliminary overview of the functions over-represented in each cluster was obtained through a KEGG pathway analysis on the overrepresented transcripts (Log2FC > 0.25) using the *C. gigas* annotation provided by the DAVID consortium (32), thereby identifying pathways specifically enriched in each cluster. Cluster 1 demonstrated enrichment in viral processing and endocytosis (**Figure 2A** and **Supplemental Table S2**). Additionally, it demonstrated enrichment in pyruvate metabolism, glycolysis/gluconeogenesis and the pentose phosphate pathways. Clusters 1 and 3 exhibited a distinctive enrichment in carbohydrate metabolism and endocytosis. In particular, cluster 3 exhibited enriched transcripts associated with glycolysis/gluconeogenesis and TCA cycle activities. Cluster 4 was enriched in protein synthesis, including transcription (spliceosome, ribosome, nucleocytoplasmic transport and mRNA surveillance pathway) folding, sorting and degradation of protein pathways. Clusters 2, 5 and 6 exhibited a shared signature of enrichment in ribosome-related genes. Cluster 2 demonstrated a specific enrichment in motor protein-coding genes responsible for cell motility and xenobiotic metabolism. Remarkably, clusters 1, 3, 4 and 5 exhibited enriched oxidative phosphorylation transcripts, whereas the transcripts of cluster 7 were enriched in vesicular trafficking and endo-lysosomal pathways (endocytosis, endosome, phagosome, lysosome, auto and mitophagy). Cluster 7 displayed also the signature of Wnt pathway components.

For a more detailed functional characterization of each transcriptomic cluster, we performed a re-annotation of the *C. gigas* genome using a combination of tools to enhance the GO term richness of the existing annotation prior to functional GO term analysis. The original annotation for *C. gigas*, based on the work of Penaloza et al. (30), provided GO annotations for 18,750 out of 30,724 genes (61%). In order to improve upon these baseline annotations, we used the *C. gigas* genome (Genbank reference GCA_902806645.1) and the associated gff3 annotation file from the Roslin Institute (30). Using the Orson pipeline (see Materials and Methods), these files were used to extract and process the longest CDSs for GO-term annotation, and we then re-annotated each predicted protein by sequence homology, assigning putative functions and improving downstream GO-term analyses. Of the 30,724 extracted CDSs, 22,462 were annotated (GO-terms and sequence description), yielding an annotation percentage of 73.1 %. Of the 30,724 CDSs, 22,391 were annotated with Molecular Functions (MF), Biological Processes (BP), and Cellular Components (CC) GO-terms (Supp. Fig. S2 and Supp. Data 2). Overall, this improved annotation coverage significantly enhances the resolution of our downstream functional analyses. Using the GO-term annotation and the Log2FC of genes calculated after scRNA-seq processing in each cluster, GO enrichment analysis was performed by rank-based gene ontology analysis (RBGOA) (33).

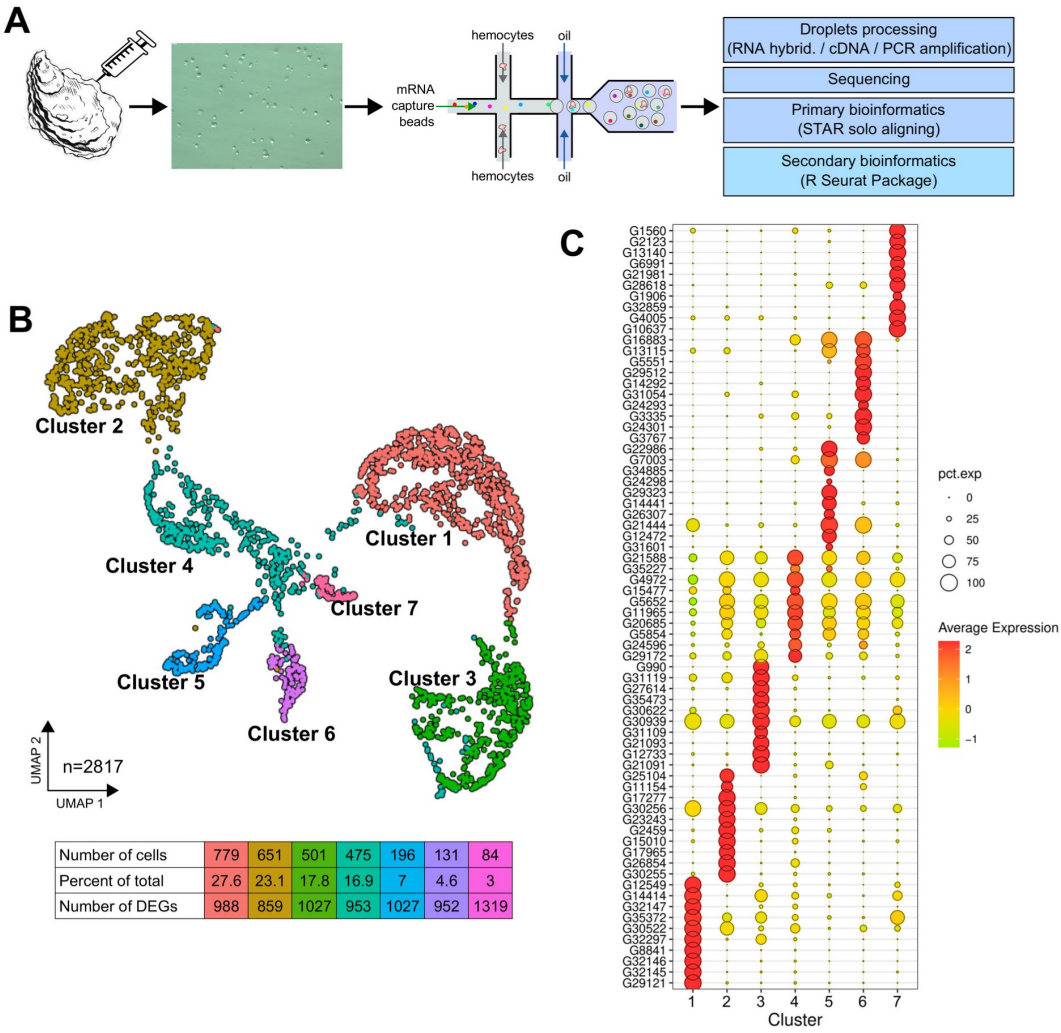

Number of cells	779	651	501	475	196	131	84
Percent of total	27.6	23.1	17.8	16.9	7	4.6	3
Number of DEGs	988	859	1027	953	1027	952	1319

Fig. 1.

scRNA-seq analysis of *C. gigas* circulating hemocytes reveals 7 transcriptomic cell clusters

(A) Schematic of the scRNA-seq 10X Genomics Chromium microfluidic technology and bioinformatics processing workflow used. Dissociated hemocytes were collected from a pathogen-free oyster and encapsulated in droplets for processing. After sequencing, the data were processed bioinformatically. **(B)** Uniform Manifold Approximation and Projection (UMAP) plot for dimensional reduction of the data set and summary of cells and the number of Differentially Expressed Genes (DEGs) in each cluster. The table shows the characteristics (number of cells, percentage of total cells and number of Differentially Expressed Genes in each cluster) of the seven clusters identified. **(C)** Dot plot representing the ten most enriched DEGs per cluster based on average expression (avg_log2FC). The color gradient of the dot represents the expression level, while the size represents the percentage of cells expressing each gene per cluster.

Gene	log2FC	Pct 1	Pct 2	Description
				Cluster 1
G29121	4.31	1	0.099	L-galactono-gamma-lactone oxidase
G32145	4.18	0.992	0.079	Angiopoietin-1 receptor
G32146	3.90	0.985	0.063	Angiopoietin-1 receptor
G8841	3.13	0.988	0.049	C-type lectin domain-containing protein
G32297	2.88	0.99	0.232	PNPLA domain-containing protein
G30522	2.76	1	0.515	Cytochrome P450 2D28
G35372	2.69	1	0.483	60S ribosomal protein L26
G32147	2.45	0.969	0.131	Angiopoietin-1 receptor
G14414	2.45	1	0.343	DUF4773 domain-containing protein
G12549	2.38	0.974	0.132	Glutaredoxin domain-containing protein
				Cluster 2
G30255	5.31	1	0.15	Metalloproteinase inhibitor 3
G26854	4.24	1	0.16	Stanniocalcin
G17965	4.21	0.94	0.04	Complement C1q-like protein 2
G15010	3.99	0.99	0.17	Kyphoscoliosis peptidase
G2459	3.82	1	0.21	*Uncharacterized protein*
G23243	3.51	0.98	0.07	Fibronectin type-III domain-containing protein
G30256	3.23	1	0.69	NTR domain-containing protein
G17277	3.21	0.99	0.04	Putative modulator of levamisole receptor-1
G11154	3.16	0.68	0.05	Collagen alpha-1(XII) chain
G25104	3.1	0.84	0.08	C1q domain-containing protein
				Cluster 3
G21091	5.51	0.99	0.13	X-box binding protein-like protein
G12733	5.42	1	0.12	Galectin
G21093	5.17	0.94	0.05	IolG
G31109	4.36	0.77	0.03	Cystatin domain-containing protein
G30939	4.25	1	0.86	Peptide ABC transporter permease
G30622	3.95	1	0.21	BHLH domain-containing protein
G35473	3.86	0.96	0.04	*Uncharacterized protein*
G27614	3.78	0.96	0.13	G Protein Receptor F1-2 domain-containing protein
G31119	3.77	0.99	0.42	Arrestin C domain-containing protein
G990	3.6	0.93	0.03	LITAF domain-containing protein
				Cluster 4
G29172	3.09	0.78	0.49	G Protein Receptor F1-2 domain-containing protein
G24596	2.37	0.78	0.25	High mobility group protein DSP1
G5854	1.8	0.64	0.38	N-acetyltransferase domain-containing protein
G20685	1.59	0.88	0.53	Ribosomal protein L22
G11965	1.57	0.92	0.7	Ribosome L4 associated C domain-containing protein
G5652	1.54	0.97	0.75	60S ribosomal protein L30
G15477	1.52	0.55	0.3	Metalloendopeptidase
G4972	1.49	0.96	0.8	60S ribosomal protein L12
G35227	1.46	0.55	0.06	ML domain-containing protein
G21588	1.42	0.94	0.69	60S ribosomal protein L13

Gene	log2FC	Pct 1	Pct 2	Description
				Cluster 5
G31601	5.24	0.38	0.06	Polyribonucleotide nucleotidyltransferase
G12472	3.99	0.85	0.03	Galectin
G21444	3.58	1	0.41	*Uncharacterized protein*
G26307	3.42	0.6	0.02	*Uncharacterized protein*
G14441	3.35	0.84	0.08	CUBN
G29323	3.21	0.9	0.01	GTPase IMAP family member 4
G24298	3.18	0.29	0.05	Putative Transmembrane protease serine 9
G34885	3.13	0.59	0.01	Gliding motility-associated C-terminal domain-containing protein
G7003	2.55	0.99	0.16	ETS-related transcription factor Elf-4
G22986	2.37	0.94	0.1	Metalloendopeptidase
				Cluster 6
G3767	6.45	0.74	0.02	Natterin-1
G24301	6.16	0.99	0.02	Aspartate-semialdehyde dehydrogenase
G3335	5.19	1	0.16	*ncRNA*
G24293	4.57	0.59	0.01	*Uncharacterized protein*
G31054	3.56	1	0.13	GATA-binding factor 3
G14292	3.29	0.87	0.03	Membrane-associated guanylate kinase inverted 3
G29512	3.2	0.99	0	Caveolin
G5551	2.93	0.97	0.02	Neuronal acetylcholine receptor subunit alpha-6
G13115	2.73	0.83	0.26	*ncRNA*
G16883	2.62	1	0.2	Allograft inflammatory factor
				Cluster 7
G10637	4.21	0.99	0.03	BZIP domain-containing protein
G4005	4.07	0.99	0.21	Ras-related protein Rab-20
G32859	3.9	0.93	0.04	G Protein Receptor F1-2 domain-containing protein
G1906	3.82	0.5	0.02	Glutathione peroxidase
G28618	3.53	0.91	0.09	Sporozoite and liver stage asparagine-rich protein
G21981	3.5	0.94	0.05	*ncRNA*
G6991	3.4	0.85	0.01	Rho-GAP domain-containing protein
G13140	3.12	1	0.03	DBH-like monooxygenase protein 1
G2123	3.05	0.94	0.02	SPRY domain-containing SOCS box protein 3
G1560	3.02	0.95	0.17	Glutathione peroxidase

Table 1.

Top 10 overexpressed genes identified in each transcriptomic cluster.

The first column indicates the gene number according to the annotation. ‘log2FC’ represents the log2 fold change of the gene in the cluster compared to all other cells. ‘Pct1’ is the percentage of cells expressing the gene in the cluster and ‘Pct2’ is the fraction of cells expressing the gene in all other clusters. The description is the annotation of the expressed gene. (adjusted p-value < 0.05).

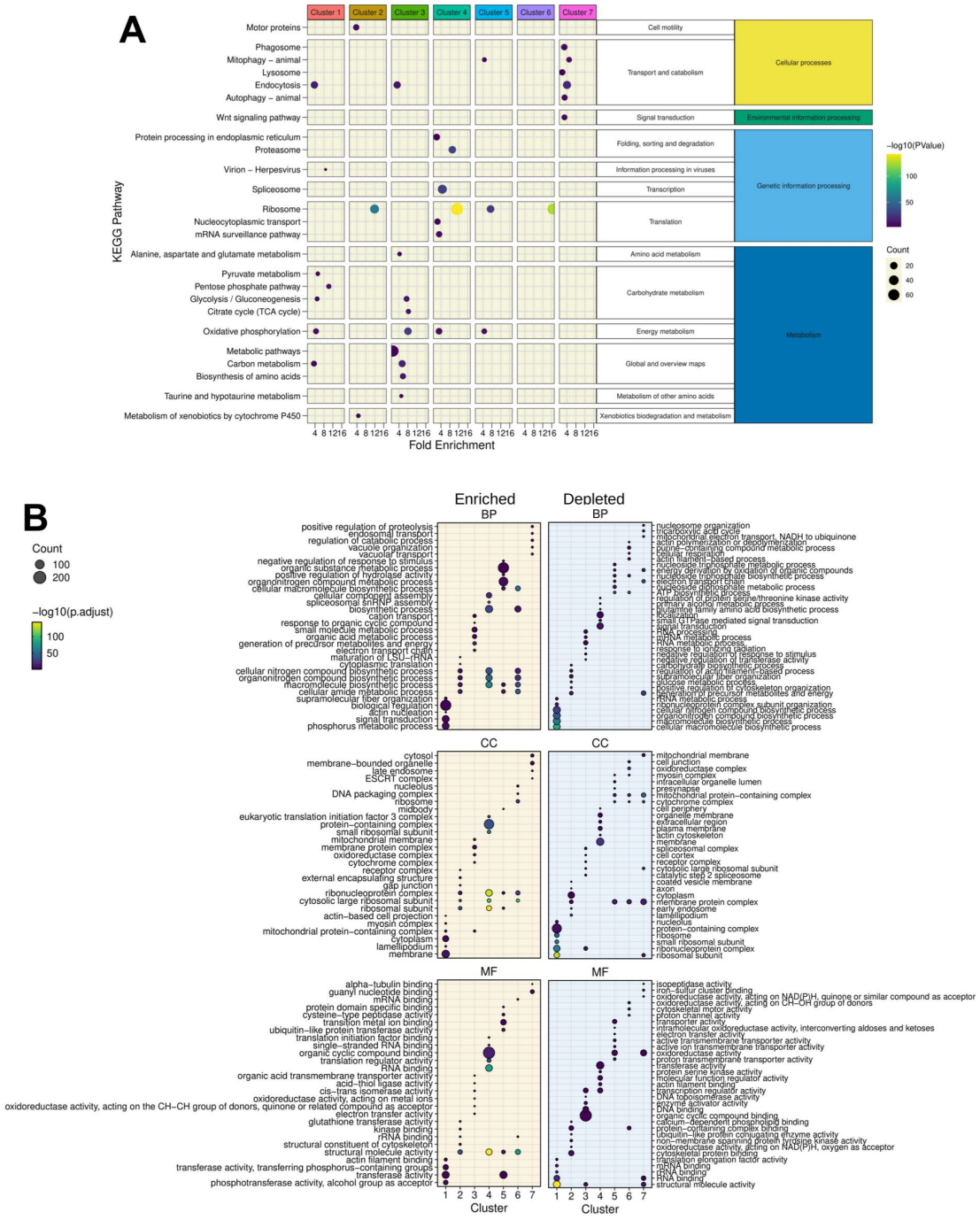

Fig. 2.

KEGG and Gene Ontology analysis of the gene signature in each cluster.

(A) A synthetic representation of the KEGG pathway analysis is shown. Colored columns represent the 7 transcriptomic clusters. Each row is a KEGG pathway, the colored dot represents the - log(p-value) and the dot size represents the number (count) of enriched genes in each pathway category. The fold enrichment is shown on the x-axis. Panels **(B)** show the results of Gene Ontology terms (GO-terms) for Biological Processes (BP), Cellular Components (CC) and Molecular Functions (MF) respectively, obtained with the genes of each cluster (Absolute value Log2FC > 0.25 and significant p-value < 0.001) using RBGOA analysis (p-value <= 0.001) for three different ontology universes. Each panel corresponds to one ontology universe, and the analysis highlights enriched and depleted terms. The dot size indicate the proportion of significant GO-terms and the gradient scale the p-adjusted value.

RBGOA analysis was performed on the GO-terms identified in each cluster (Supp. Data 3). The results are presented in **Figure 2B**. The scRNA-seq-based analysis identified seven distinct transcriptomic profiles for each cell cluster, thereby shedding light on greater heterogeneity and functional diversity of *C. gigas* hemocytes than previously described. Cluster 1, comprising 27.6 % of cells, is characterized by GO-terms related to myosin complex, lamellipodium, membrane and actin cytoskeleton remodelling, as well as phosphotransferase activity. This is evidenced by an enrichment in actin nucleation, phosphorus metabolic process and signal transduction BP, actin filament binding and phosphotransferase activity MF and lamellipodium and actin-based cell projection CC. Cluster 2, comprising 23.1 % of cells, has an increased translation activity, as indicated by enrichment in BP, MF and CC terms related to rRNA binding, cytoplasmic translation, maturation of LSU-rRNA, and ribosomes respectively. Cluster 3, representing 17.8 % of cells, shows enrichment in cellular oxidation and actin nucleation, as evidenced by an enrichment in BP and MF related to oxidoreductase activities acting on metal ions, electron transfer and cellular oxidation, and CC related to cytochromes, oxidoreductase complex, and mitochondrial protein-containing complexes. Cluster 4, representing 16.9 % of cells, has transcriptomic signatures reminiscent of spliceosome assembly, RNA maturation, and macromolecules biosynthesis (BP related to biosynthetic process, macromolecules biosynthesis process, and spliceosome assembly, MF related to RNA and ssRNA binding and translation initiation, and CC related to ribosomes and ribonucleoprotein complexes). Cluster 5, comprising 7 % of cells, demonstrates enrichment in structural molecule activity, hydrolase regulation and ubiquitin-like protein transferase activity, as evidenced by its BP, MF, and CC related to ribosome and midbody localization. Cluster 6, comprising 4.6 % of cells, is characterized by a specific nucleosome organization, translation, and biosynthetic processes, with related BP, MF, and CC tied to nucleolus, ribosomes, ribonucleoprotein complex and rRNA binding. Cluster 7, representing a mere 3 % of cells, is characterized by multivesicular body sorting, vacuolar transport, vacuole organization, and positive regulation of proteolysis, with related BP, MF, and CC of the ESCRT machinery.

Seven morphologically distinct immune cell types are identified by quantitative cytology and transcriptomic markers

Cytological studies were conducted using MCDH staining to better characterize the diversity of circulating hemocytes in *C. gigas*. Seven distinct hemocyte morphotypes were identified: three non-granular (acidophilic blasts, basophilic blasts and hyalinocytes) and four granular (small granule cells, big granule cells, vesicular cells and macrophage-like) (**Fig. 3** and **Supp. Fig. S3**). Hyalinocytes (30 % of total hemocytes) are large cells with an irregular spreading membrane. They contain an azurophilic cytoplasm without granulations and their irregular nucleus varies in size (**Fig. 3A panel H**). Basophilic blasts characterized by a basophil cytoplasm (**Fig. 3A panel BBL**) and acidophilic blasts with acidophil cytoplasm (**Fig. 3A panel ABL**) accounted for 17 % and 14 %, respectively, of the total hemocytes. They are rounded cells without granulation, with a uniform and regular dense nucleus and a high nucleo-cytoplasmic ratio. Macrophage-like cells (20 % of the hemocytes) present an irregular membrane punctuated by rare pseudopodia with a polylobed nucleus and a basophilic cytoplasm where polychromatic inclusions of various sizes could be observed (**Fig 3A. panel ML**). Small granule cells (13 % of total hemocytes) have an irregular membrane punctuated by rare pseudopodia, an acidophilic cytoplasm, and numerous homogeneous purple granules (**Fig. 3A panel SGC**). Big granule cells (4 % of total hemocytes) are rounded cells with a basophilic cytoplasm containing large, slightly dark purple to black vesicles of heterogeneous size (**Fig. 3A panel BGC**). Vesicular cells (2 % of total hemocytes) are rounded cells with acidophilic cytoplasm, rich in homogeneous transparent and fluorescent to UV light vesicles with an irregular nucleus (**Fig. 3A panel VC**). Only blasts (BBL, ABL) have a nucleo-cytoplasmic ratio greater than 0.6, whereas the other hemocytes described have a nucleo-cytoplasmic ratio less than 0.3.

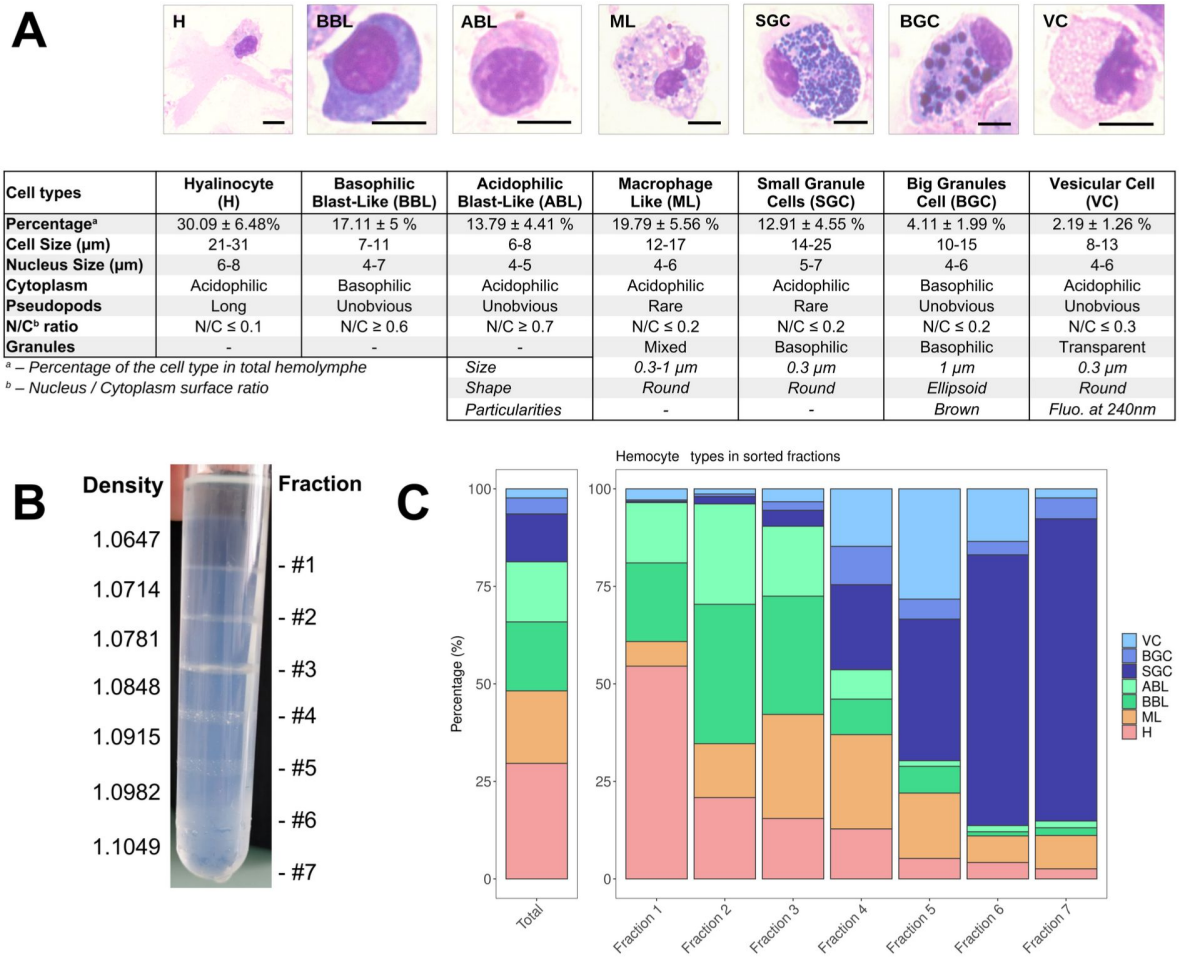

Cell types	Hyalinocyte (H)	Basophilic Blast-Like (BBL)	Acidophilic Blast-Like (ABL)	Macrophage Like (ML)	Small Granule Cells (SGC)	Big Granules Cell (BGC)	Vesicular Cell (VC)
Percentage[a]	30.09 ± 6.48%	17.11 ± 5 %	13.79 ± 4.41 %	19.79 ± 5.56 %	12.91 ± 4.55 %	4.11 ± 1.99 %	2.19 ± 1.26 %
Cell Size (µm)	21-31	7-11	6-8	12-17	14-25	10-15	8-13
Nucleus Size (µm)	6-8	4-7	4-5	4-6	5-7	4-6	4-6
Cytoplasm	Acidophilic	Basophilic	Acidophilic	Acidophilic	Acidophilic	Basophilic	Acidophilic
Pseudopods	Long	Unobvious	Unobvious	Rare	Rare	Unobvious	Unobvious
N/C[b] ratio	N/C ≤ 0.1	N/C ≥ 0.6	N/C ≥ 0.7	N/C ≤ 0.2	N/C ≤ 0.2	N/C ≤ 0.2	N/C ≤ 0.3
Granules	-	-	-	Mixed	Basophilic	Basophilic	Transparent
Size				*0.3-1 µm*	*0.3 µm*	*1 µm*	*0.3 µm*
Shape				*Round*	*Round*	*Ellipsoid*	*Round*
Particularities				-	-	*Brown*	*Fluo. at 240nm*

[a] – *Percentage of the cell type in total hemolymphe*
[b] – *Nucleus / Cytoplasm surface ratio*

Fig 3.

C. gigas naive hemocyte formula and Percoll gradient hemolymph fractionation

(A) Morphology, percentages and characteristics of the 7 cell types identified by MCDH staining. **H** : Hyalinocyte, **ML** : Macrophage Like, **BBL** : Basophilic Blast Like cell, **ABL** : Acidophilic Blast Like cell, **SGC** : Small Granule Cell, **BGC** : Big Granule Cell, **VC** : Vesicular Cell. Scale bar : 5 µm. For the ML, SGC, BGC, and VC hemocyte types, size refers to the average granule diameter, shape describes the morphology of the granules (e.g., round, ellipsoid), and particularities highlight distinguishing features such as granule color or fluorescence properties observed under specific staining or imaging conditions. **(B)** Sorting of hemocytes on a discontinuous Percoll gradient. 7 fractions were identified along the gradient at the top of each density cushion (from d=1.0647 at #1 to d= 1.1049 at #7). **(C)** Representation of the average values (from 5 different fractionation experiments) of the different hemocyte types in the seven percoll gradient fractions compared to the average hemolymph composition of a naive oyster (Total). **VC** : Vesicular Cells, **BGC** : Big Granule Cells, **SGC** : Small Granule Cells, **ABL** : Acidophilic Blast Like cells, **BBL** : Basophilic Blast Like cells, **ML** : Macrophage Like cells and **H** : Hyalinocytes respectively. (**Supp. Fig. S4** for statistics).

To gain further insight into the functional characterization of these diverse hemocyte morphotypes and to associate them with the transcriptomic clusters identified in the scRNA-seq, we enhanced an existing hemocyte fractionation approach using an isopycnic Percoll density gradient to sort the hemocytes (34). Cell sorting was performed using a discontinuous Percoll gradient with densities ranging from 1.0647 to 1.1049. Seven distinct density fractions were established (**Fig. 3B**) and the hemocyte composition was then characterized by cytological analysis of each fraction (**Fig. 3C**; see also **Supp. Fig. S4** for statistical significance). The uneven distribution of hemocyte morphotypes along the density gradient enabled a relative separation of the different cell populations (**Supp. Fig S4**). In summary, hyalinocytes were significantly enriched in the first fraction, while macrophage-like cells were significantly enriched in fraction 3 and fraction 4. Acidophilic blasts were significantly enriched in fraction 2. Basophilic blasts were significantly enriched in fractions 2 and 3. Vesicular cells were enriched in fraction 5, big granule cells were enriched in fraction 4 and small granule cells in fractions 6 and 7 (**Fig. 3C** and **Supp. Fig. S4**).

To identify the transcriptomic cell clusters corresponding to the different hemocyte morphotypes, we used RT-qPCR to detect the expression of different cluster-specific marker genes in the different hemocytes in the Percoll density fractions. The marker genes were selected without any a priori assumptions based solely on their enrichment levels (Log2C) and their percentage of expression (Pct1 / Pct2 ratio)F in the cluster of interest relative to all other cell clusters (**Table 2**). The expression level of each marker in the seven different clusters confirmed that the 14 selected marker genes were differentially expressed in each scRNA-seq transcriptomic cluster (**Supp. Fig. S5**).

RT-qPCR expression profiles in the hemocyte fractions obtained from the Percoll density gradient revealed distinct patterns according to the different transcriptomic cluster marker genes (**Fig. 4A**). Cluster 1 markers (LACC24 and CLEC) were overexpressed in fractions 1, 2, 3 and underexpressed in the remaining fractions relative to total hemocytes. Cluster 2 markers (EGFL and LEVAR) showed a decreasing pattern of expression from fraction 1 to fraction 7. Cluster 3 markers (TGC and XBOX) showed a significant increase in expression in fractions 4 to 7. Cluster 4 markers (MLDP and HMGB1) showed a gradually decreasing expression pattern from fraction 2 to fraction 7. Cluster 5 marker genes (GAL and CUBN) were underexpressed in fractions 4 to 7, but not differentially expressed in fractions 1 to 3 compared to total hemocytes. Cluster 6 marker genes (CAV and NAT1) were overexpressed in fraction 3, expressed similarly to total hemocytes in fraction 2, and underexpressed in fractions 1, and 4 to 7. Finally, cluster 7 marker genes (MOX and GPROT) were overexpressed only in fractions 3 to 7. Correlation analysis and statistical validation demonstrated a clear association between hemocyte morphotypes and 14 gene markers (**Fig. 4B**, **Fig. 4C** and **Supp. Table S4**). Cluster 3 marker genes (TGC and XBOX) correlated positively (r = 0.74 & 0.75) and specifically with small granule cells (SGC). Cluster 7 markers (MOX and GPROT) correlated (r = 0.68 and r = 0.56) with vesicular cells (VC). Cluster 2 markers (EGFL and LEVAR) correlated positively with hyalinocytes (H) (r=0.85 and r=0.81). No specific markers could be identified for blasts and macrophage-like cells.

By employing RT-qPCR, cell sorting on Percoll gradients, and scRNA-seq analysis, we could identify cell types corresponding to three transcriptomic clusters. Cluster 3 corresponds to small granule cells (SGC), cluster 2 to hyalinocytes (H), and cluster 7 to vesicular cells (VC). Cluster 3, cluster 2 and cluster 7 represent 17.8 %, 23 % and 3 % of the total cells analyzed by scRNA-seq, respectively. This is consistent with cytological data, which indicated the presence of 12.5 % +/-5 % Small Granule Cells, 30 % +/-9.3 % Hyalinocytes and 2.3 % +/-1.6 % Vesicular Cells (**Fig. 1B** and **Fig. 3A**). Furthermore, the molecular and cellular functions derived from GO-term and KEGG analyses (**Fig. 2**) were in alignment with the anticipated functions for these three cell types.

Gene Number	Avg. Log2FC	Pct.1	Pct.2	Pct.1/Pct.2 Ratio	Cluster	Description	Marker Name
G8994	2.05	0.917	0.024	38.20	1	Laccase-24	LACC24
G8841	3.13	0.988	0.049	20.16		C-type lectin domain-containing protein	CLEC
G24846	2.31	0.914	0.029	31.52	2	EGF-like domain-containing protein 8	EGFL
G17277	3.21	0.989	0.043	23.00		Putative modulator of levamisole receptor-1	LEVAR
G22387	3.16	0.972	0.029	16.76	3	TGc domain-containing protein	TGC
G21091	5.51	0.992	0.129	7.69		X-box binding protein-like protein	XBOX
G35227	1.46	0.549	0.055	9.98	4	ML domain-containing protein	MLDP
G31074	0.94	0.501	0.077	6.51		High mobility group protein B1	HMGB1
G14441	3.35	0.837	0.076	11.01	5	Cubilin	CUBN
G12472	3.99	0.847	0.034	24.91		Galectin	GAL
G29512	3.20	0.985	0.004	246.25	6	Caveolin	CAV
G3767	6.45	0.740	0.018	41.11		Natterin-1	NAT1
G13140	3.12	1.000	0.025	40.00	7	DBH-like monooxygenase protein 1	MOX
G32859	3.90	0.929	0.039	23.82		G protein receptor F1-2 domain-containing protein	GPROT

Table 2.

Table of the 14 marker genes specific to the different transcriptomic clusters.

Gene number, average Log2FC, pct1/pct2 ratio (percentage of cells expressing this transcript in the cluster divided by the percentage of all other cells expressing this transcript) and cluster number are reported. The description is taken from our annotation and the marker name is derived from the description.

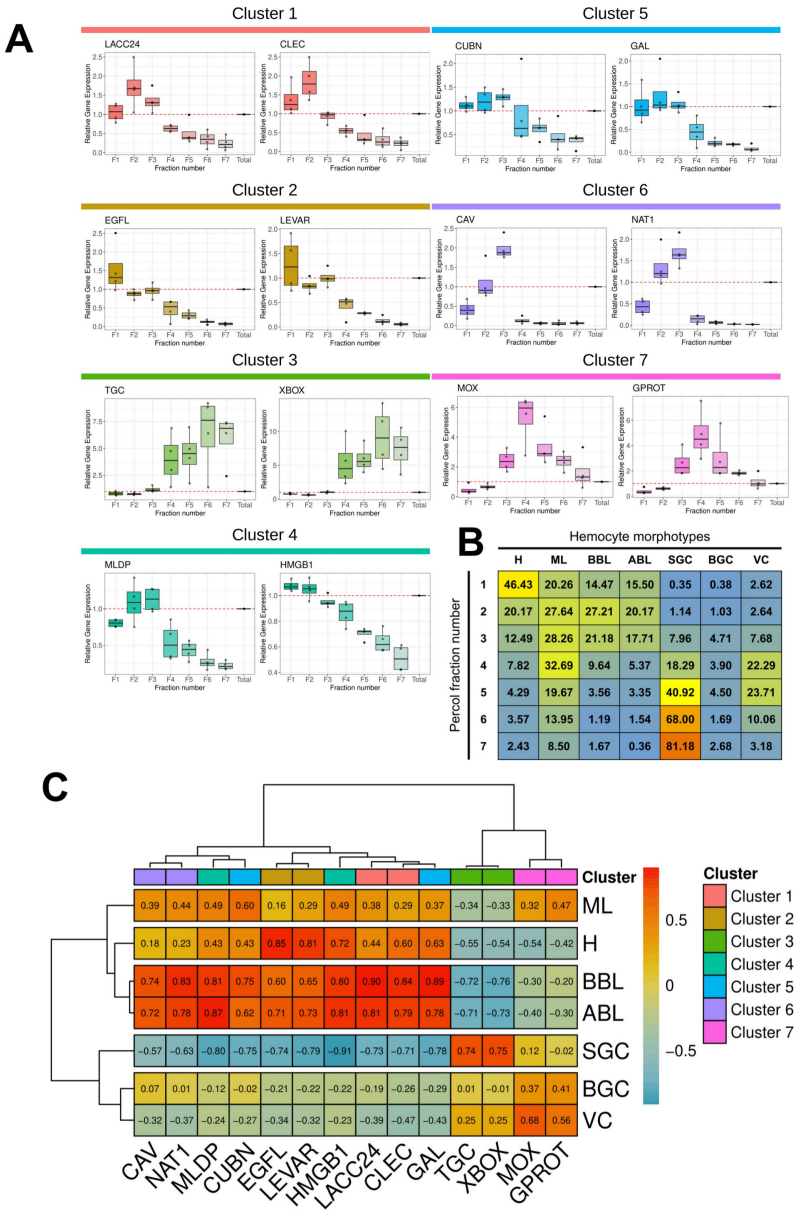

Fig 4.

Characterization of molecular markers specific to the different hemocyte morphotypes.

(A) Relative gene expression level of the 14 markers in the various fractions after gradient density sorting. The graphs show the relative expression of genes compared to their expression in total hemocytes in the various fractions (red dotted line). Relative gene expression levels were normalized to the reference gene Cg-rps6 and the $2^{-\Delta Ct}$ method was used to calculate relative expression levels, where ΔCt represents the difference between the target gene's Ct value and the reference gene's Ct value. Standard deviations were calculated based on four independent experiments. **(B)** Average percentage of each hemocyte type in the 7 Percoll gradient fractions used to quantify marker gene expression by qPCR. **(C)** Correlation matrix between the relative gene expression of each marker gene in each fraction and the percentage of each hemocyte type in the same fractions. Values and color scale represent the Pearson correlation coefficient (r) ranging from -1 (inverse correlation) to +1 (full correlation). **H** : Hyalinocyte, **ML** : Macrophage Like, **BBL** : Basophilic Blast Like cell, **ABL** : Acidophilic Blast Like cell, **SGC** : Small Granule Cell, **BGC** : Big Granule Cell, **VC** : Vesicular Cell. **LACC24** : Laccase 24, **CLEC** : C-type lectin domain-containing protein, **EGFL** : EGF-like domain-containing protein 8, **LEVAR** : Putative regulator of levamisole receptor-1, **TGC** : TGc domain-containing protein, **XBOX** : X-box binding protein-like protein, **MLDP** : ML domain containing protein, **HMGB1** : High mobility group protein B1, **CUBN** : Cubilin, **GAL** : Galectin, **CAV** : Caveolin, **NAT1** : Natterin-1, **MOX** : DBH-like monooxygenase protein 1, **GPROT** : G protein receptor F1-2 domain-containing protein.

Only macrophage-like and small granule cells behave as professional phagocytes

The hemocytes separated on the Percoll gradient were characterized functionally to gain further insight into their functional specialization. Two hemocyte functions, namely phagocytosis and production of Reactive Oxygen Species (ROS), are known to carry out major cellular antimicrobial activities. Granular cells have been suggested to be the professional phagocytes specialized for these functions (22). Phagocytosis and oxidative burst were studied using cell response toward zymosan particles (35).

The phagocytic activity of hemocytes was first tested on a sample of total oyster hemolymph. Cells were incubated for 1 hour with either zymosan particles or the bacterial strain *Vibrio tasmaniensis* LMG20012^{T}. Only the small granule cells and the macrophage-like cells exhibited efficient phagocytosis for both zymosan or vibrios, as observed after MCDH staining (**Fig. 5A**, **Supp. Fig. 6 and Supp. Fig. 7A**). Macrophage-like cells and small granule cells showed a phagocytic activity of 49 % and 55 %, respectively, and a phagocytosis index of 3.5 and 5.2 particles per cell respectively (**Fig. 5B** and **Supp. Fig. 7B**), as confirmed in 3 independent experiments examining a total of 2,807 cells. Very limited phagocytic activity was observed for hyalinocytes (1.7 %), basophilic blasts (0.18 %), and big granule cells (2.7 %) with a phagocytosis index of 2, 1, and 2.5 particles per cell, respectively (**Fig. 5B** and **Supp. Fig. 7B**). These results confirmed that only small granule cells and macrophage-like cells behave as professional phagocytes demonstrating robust phagocytic activity.

Only macrophage-like cells produce Reactive Oxygen Species

The next step was to assess the capacity of *C. gigas* hemocytes in each Percoll fraction to produce Reactive Oxygen Species (ROS) upon stimulation by zymosan, utilizing the Luminol oxidation assay. Luminol luminescence peaked 25 minutes after exposure of hemocytes (isolated from total hemolymph) to zymosan, indicating a robust oxidative burst (**Fig. 5C**). The production of ROS was dependent on a NADPH oxidase, as it was completely inhibited by the NADPH oxidase-specific inhibitor apocynin (**Fig. 5D**). To ascertain which hemocyte types were involved in ROS production we tested Percoll density-sorted hemocytes for oxidative burst activity. Fractions 2 and 3 displayed higher oxidative burst activity than the other fractions. The burst intensity of fraction 3 was twice that of total hemocytes, and fraction 2 also exhibited significantly increased burst activity. In contrast, fraction 4 showed a significant decrease in oxidative burst, and no activity was observed for fractions 1, 6 and 7 (**Fig. 5D**). These results indicate that NADPH-dependent oxidative burst activity is carried out by fractions enriched in macrophage-like (ML) cells and blast-like cells (ABL and BBL).

Previous studies have shown that granular cells can produce ROS (22). In contrast, we found that small granule cells collected in fraction 7 could not produce ROS through an oxidative burst. To identify which type of hemocyte from blast-like cells and macrophage-like cells produces ROS within a few minutes after exposure to zymosan, ROS production was investigated using NitroBlueTetrazolium (NBT) reduction to stain hemocytes directly. Correlative microscopic analysis using MCDH staining can then be conducted after the NBT reduction reaction. Macrophage-like cells were strongly and significantly stained by NBT reduction (33.2 %) (**Fig. 5E, panels a & d**). In contrast, some small granule cells were lightly stained by NBT reduction (**Fig. 5F**). Blast-like cells, big granule cells, vesicular cells, and hyalinocytes were never NBT stained, confirming that these cell types were not involved in ROS production (**Supp. Fig. S7**). Taken together, these observations demonstrate that small granule cells and macrophage-like cells are the two professional phagocytes among hemocytes. However, only macrophage-like cells are capable of oxidative burst upon exposure to zymosan. In light of these new functional data, we further analyzed the expression level of NADPH-oxidase-related enzymes in the scRNA-seq

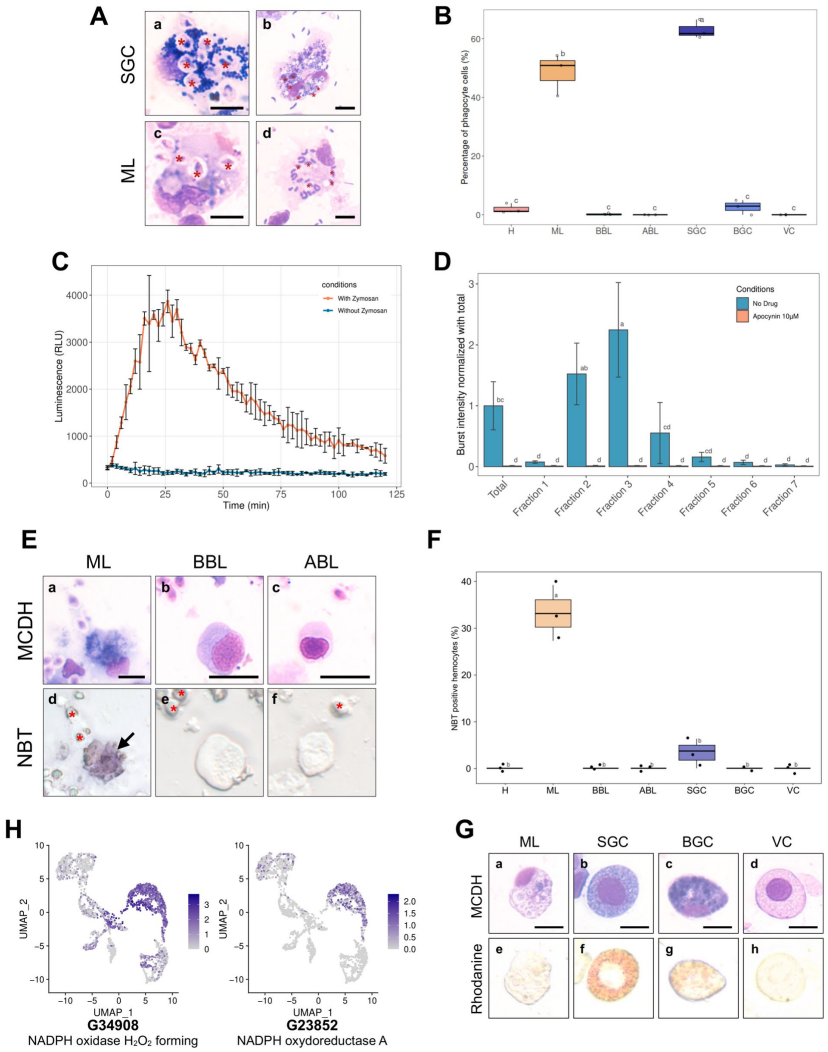

Fig 5.

Phagocytosis, Reactive Oxygen Species production capacity and copper storage of hemocytes.

(A) Images of small granule cells (**SGC**) and macrophage-like (**ML**) cells with phagocytosed zymosan particles (**panels a & c - red stars**) and *Vibrio tasmaniensis* LMG20012^T bacteria (**panels b & d - red stars**) from whole hemolymph sample. Scale bar : 5 µm. **(B)** Quantification of the phagocytic activity of zymosan particles by each cell type. The graph shows the result of 3 independent experiments. **(C)** Luminescence recording to detect the production of Reactive Oxygen Species (ROS). In orange, a biphasic curve was obtained on naive oyster hemolymph after zymosan addition at t = 0 min. In blue, the control condition corresponds to hemocytes without zymosan addition. **(D)** Graph showing the intensity of ROS production in each Percoll fraction. Normalized burst intensity was calculated from the luminescence peak obtained from each fraction. In blue, no drug was added to the experiment, in orange, ROS production was impaired by the addition of apocynin. **(E)** NBT (NitroBlueTetrazolium) staining of hemocytes exposed to zymosan particles. Hemocytes morphology after MCDH staining: Macrophage Like **(a)**, Basophilic **(b)** and Acidophilic **(c)** Blast cells. NBT staining of the different types of hemocytes **(d-f)**. Red stars show zymosan and bacteria particles. Black arrows indicate Macrophage-Like cells. Scale bar : 10 µm **(F)** Quantification of NBT-positive cells present in the total hemolymph of oysters exposed to zymosan. **(H)** UMAP plots showing cells expressing NADPH oxidase found in the scRNA-seq dataset and their expression level. **(G)** Labeling of intracellular copper stores in *C.gigas* hemocytes. MCDH (upper panels) and rhodanine (lower panels) staining of oyster hemocytes to reveal copper accumulation. Scale bar : 10µm. For panels **(B)**, **(D)** and **(F)** the alphabetic characters displayed above the data points in each plot represent statistically significant differences among the groups, as determined by Tukey's test following ANOVA. Groups denoted by different letters differ significantly at the $p < 0.05$ level of statistical significance. **H** : Hyalinocytes, **ABL** : Acidophilic Blast-Like cells, **BBL** : Basophilic Blast-Like cells, **ML** : Macrophage-Like cells, **SGC** : Small Granule Cells, **VC** : Vesicular Cells and **BGC** : Big Granule Cells.

dataset. The cells in cluster 1 predominantly expressed two NADPH oxidase isoforms (gene numbers G34908 and G23852) compared to other clusters (**Fig. 5H**). Furthermore, this cluster expresses macrophage-related genes, including the macrophage-expressed gene 1 protein (G30226) (**Supp. Data S1**), along with maturation factors for dual oxidase, an enzyme involved in peroxide formation (**Supp. Fig. S8**), supporting its designation as macrophage-like based on functional characteristics. Collectively, these data indicated that cells of transcriptomic cluster 1 corresponded to macrophage-like cells.

Small granule cells and big granule cells accumulate intracellular copper

The effects of copper on oyster hemocytes have been studied extensively due to its abundance in polluted marine environments (19). In addition, several studies have shown that *Vibrio* species pathogenic for *C. gigas* possess copper resistance genes, which are crucial for their survival within hemocytes (9). This prompted us to investigate which hemocyte types are involved in copper metabolism. To this end, total hemocytes were isolated from naive oysters and stained with rhodanine to reveal copper storage in cells, and a total of 1,562 cells were examined across three independent experiments. Rhodanine staining revealed that 33 % +/-2 % of small granule cells and 30 % +/-10 % of big granule cells exhibited a specific reddish/brown staining indicative of a high concentration of copper in their granules (**Fig. 5G** and **Supp. Fig. S9**). These results provide functional evidence that small granule cells (SGCs) are specialized in metal homeostasis in addition to phagocytosis, as suggested by the scRNA-seq data identifying cluster 3. Specifically, single-cell RNA sequencing revealed an upregulation of copper transport-related genes, including G4790 (a copper transporter) with a 2.7 log2FC and a pct ratio of 42, reinforcing the role of SGCs in copper homeostasis (see **Supp. File S1**).

Antimicrobial peptides are expressed by agranular cells, blasts and hyalinocytes

Antimicrobial peptides (AMPs) have long been studied for their role in the invertebrate humoral immune response. They are expressed by hemocytes, including those in *C. gigas* (36). The aim was to ascertain whether different hemocyte cell types expressed distinct AMPs. However, due to the limited sequencing depth, the scRNA-seq analysis was not sensitive enough to reveal AMP expression. This limitation was addressed by investigating AMP expression through RT-qPCR on Percoll density-fractionated hemocytes. The results indicated that Cg-Bigdefs 1-2, Cg-BPI and hemocyte defensin were predominantly expressed by agranular cells, blasts and hyalinocytes (ABL, BBL and H) (**Fig. 6A, B** and **C**). The expression of these AMPs was associated with Blasts abundance, while the expression of Cg-BigDefs 1-2 was only associated with hyalinocytes (**Fig. 6D**). Granular cells (VC, ML, BGC and SGC) did not seem to express any of the analyzed AMPs. These data suggest that some of the agranular cells are specialized in the production of humoral effectors.

Tentative model of hemocyte lineages and differentiation pathways in *C. gigas*

The ontogeny, lineage and differentiation pathways of bivalves remain largely unknown (37). However, there are some indications of circulating and proliferating hemocyte progenitors in the hemolymph of *C. gigas* (38). GO-terms analysis of the 7 transcriptomic clusters revealed different functional signatures, including the transcriptomic signature of cluster 4, which showed a high expression level of ribosomal proteins (Supp. Fig. S1J) . This particularity has been observed in hematopoietic stem cells in vertebrates (39–41). Furthermore, scRNA-seq approaches using bioinformatic tools like Monocle3 (42) can now be used to deduce differentiation pathways from trajectory inference using gene expression profiles analysis. This

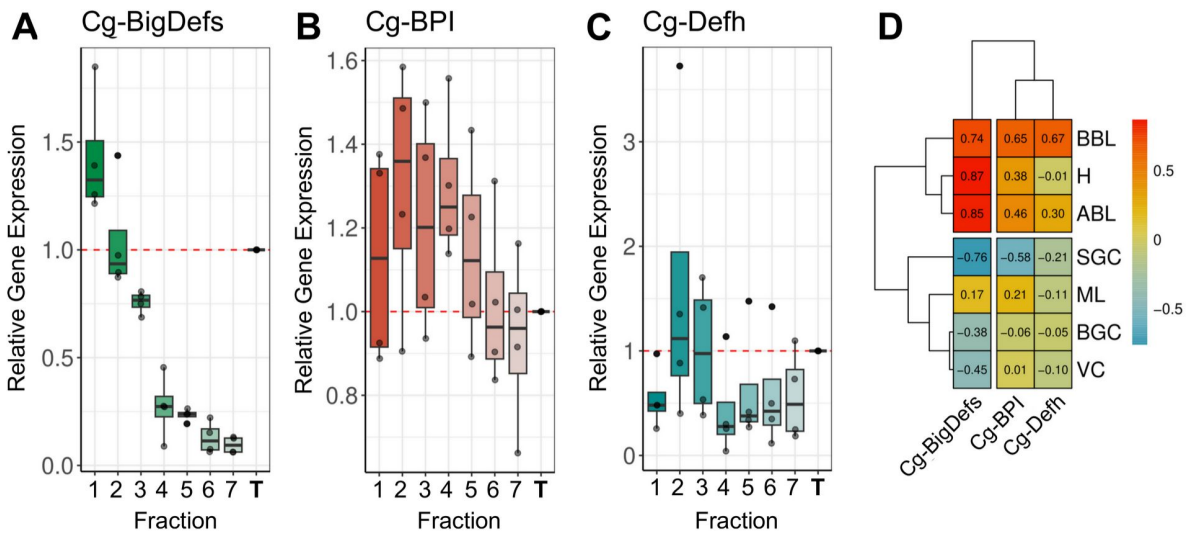

Fig 6.

Hemocyte expression profiles of some antimicrobial peptides.

(A) (B) and **(C)** Relative gene expression in the 7 Percoll hemocyte fractions of Big-Defensin1 & 2 (Cg-BigDefs), BPI (Cg-BPI) and hemocyte defensin (Cg-Defh), respectively, in comparison to the gene expression level in unfractionated hemolymph. Relative gene expression levels were normalized to the reference gene Cg-rps6. The $2^{-\Delta Ct}$ method was used to calculate relative expression levels, where ΔCt represents the difference between the target gene's Ct value and the reference gene's Ct value. **(D)** Correlation matrix between the relative gene expression of BigDefensin1 & 2, BPI and hemocyte defensin gene in each fraction and the percentage of each hemocyte type in each fraction (**H** : Hyalinocytes, **ABL** : Acidophilic Blast Like, **BBL** : Basophilic Blast Like, **SGC** : Small Granule Cell, **ML** : Macrophage Like, **BGC** : Big Granule Cell, **VC** : Vesicular Cell. Values and color scale represent the Pearson correlation coefficient (r) ranging from -1 (inverse correlation) to +1 (full correlation).

revealed an overrepresentation of functions involved in the splicing, transcription and translation continuum in the same fourth cluster (see cluster 4 in **Fig. 2A** and **Fig. 2B**), thereby supporting the hypothesis of a pool of quiescent or immature cells that can differentiate upon stimulation.

Cluster 4 was chosen to enroot the pseudotime analysis to deduce differentiation pathways and cell lineages using Monocle3. (**Fig. 7A**). By temporally ordering the 2817 cells analyzed by scRNA-seq, 6 cell lineages could be defined (**Fig. 7B**). Differentiation pathway 1 leads to hyalinocytes (H) (**Fig. 7C**). This transition is characterized by the downregulation of 11 genes (**Supp. Fig. S10A**), two of which are transcription factors (G31522 and G7003). The hyalinocyte cluster was also characterized by the overexpression of genes involved in cell contractility (G11418, G22824, G153 and G718). Differentiation pathway 2 leads to cells of cluster 5 and is characterized by the upregulation of about 26 genes (**Supp. Fig. S10B**), one gene related to metalloendopeptidase activity (G15477) was downregulated, a GTPase IMAP gene (G29323) and three transcription factors were upregulated (G7003, G11013 and G4646) (**Fig. 7D**). Differentiation pathway 3 leads to cells of cluster 6 and is characterized by the upregulation of 22 genes (**Supp. Fig. S10C**). Three fibrinogen-related protein genes (G20176, G20226 and G20227) and a GATA-binding factor (G31054) were up-regulated whereas a metalloendopeptidase gene (G15477) was downregulated. The severin gene displayed a transient increased expression (G28864) (**Fig. 7E**). The pathways between clusters 4, 5 and 6 found by Monocle3 analysis were pseudo temporally short and few specific markers were identified, suggesting that they were transcriptionally close. Differentiation pathway 4 leads to vesicular cells (VC) (**Fig. 7F**) where a large number of genes were activated to give rise to these cells (**Supp. Fig. S10D**). Four genes were specifically downexpressed in VC (G15477, G25512, G2213 and G29172). Interestingly, 6 genes encoding potential transcription factors were upregulated in this lineage (G30997, G10637, G1067, G13555, G2123 and G27827). Differentiation pathway 5 leads to macrophage-like cells (ML), and is characterized by the underexpression of 41 genes and the overexpression of 20 genes (**Supp. Fig. S10E**). Among the 41 genes, 6 are putative transcription factors (G2123, G10637, G13555, G27827, G1067 and G11196) (**Fig. 7G**). Finally, we can outline a lineage ending in small granule cells (SGC) (**Fig. 7H**). This pathway involved cluster 4 (immature cells), VC, ML and SGC and was characterized by the downregulation of 27 genes (**Supp. Fig. S10F**), including 5 potential transcription factors (G10637, G13555, G27827, G1067 and G2123). SGC showed a distinct transcriptomic signature with 61 overexpressed genes, including 3 transcription factors (G1708, G21091 and G30622). Based on these findings, we postulate that immature cluster 4 cells possess pluripotent potential and can give rise to four terminally differentiated cell types : cluster 5 and 6 cells, hyalinocytes and small granule cells, and two other transient hemocyte cell types : vesicular cells and macrophage-like cells. All data from the Monocle3 analyses are available as Supplementary Data (**Supp. Fig. S10**).

Differentiation pathway analysis thus revealed the over- or under-expression of various transcription factors in the identified pathways. Given the established role of transcription factors as master regulators of cell differentiation and their utility in delineating cell lineages, we investigated the combinatorial expression patterns of transcription factors among the different transcriptomic cell clusters. Based on GO-terms annotation, 28 different sequences corresponding to transcription factors were isolated from the scRNA-seq dataset. The transcription factor function was confirmed by manual annotation (**Supp. Table S5**) and **Figure 7I** shows the average expression profiles of these factors in the different clusters. **Supplementary Figure S11** illustrates their expression levels in single cells. Two transcription factors, CgATF5 and CgCRBL1, exhibited a contrasting expression profile with an increased average expression in macrophage-like cells, hyalinocytes and small granule cells versus a low expression profile in cells in clusters 4, 5, 6 and vesicular cells. We also identified transcription factors that were specifically expressed in the different transcriptomic clusters : CgSPDEF, CgSOCS3, CgFOS and CgTFEB were specific for vesicular cells, CgSOX8, CgXBOX and CgELF3 were specific for small granule cells, CgCR3L1 and CgTAL1 for hyalinocytes, and CgJUN, CgKLF5, CgKLF6 and CgCREM for macrophage-like cells. Eight

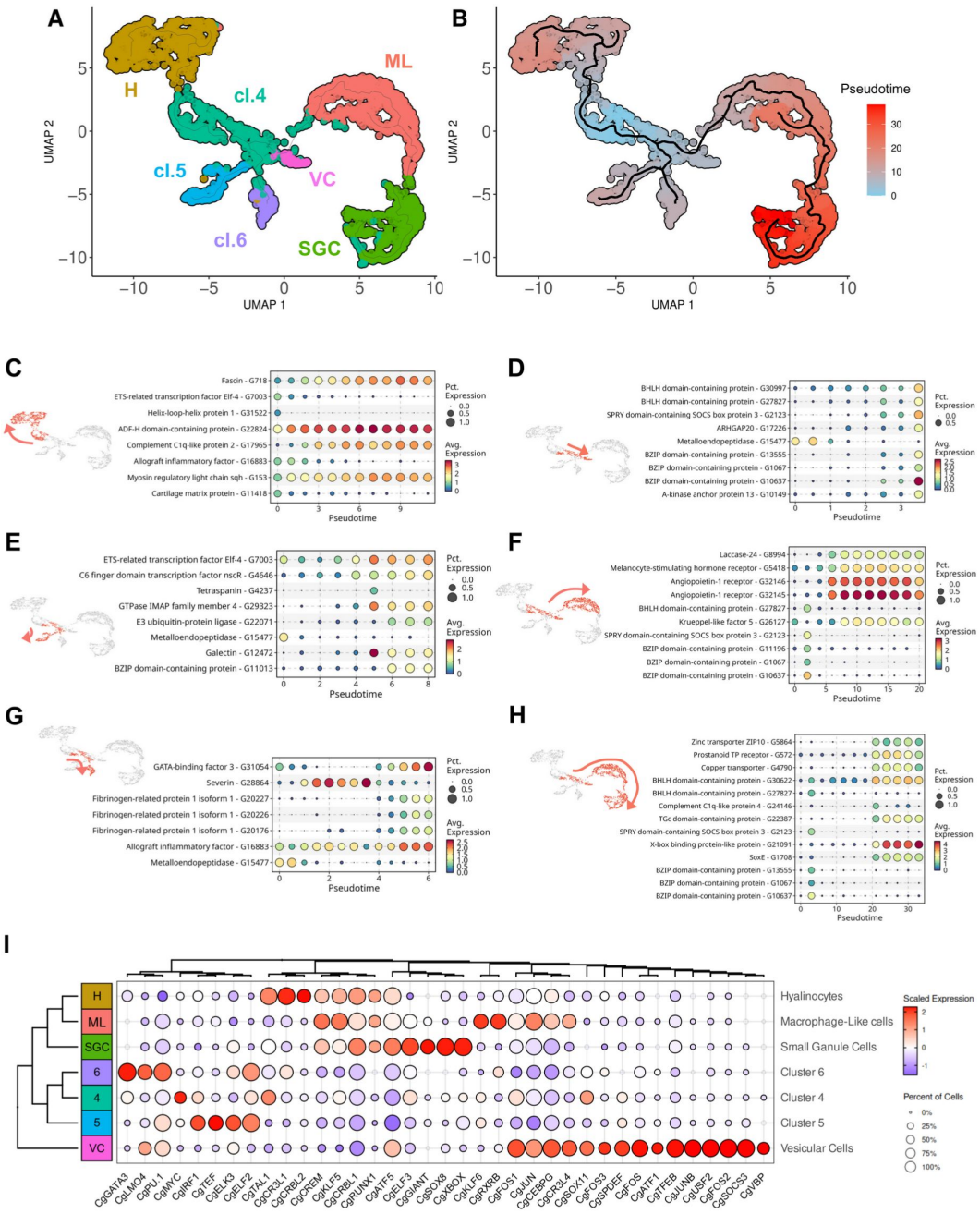

Figure 7.

Pseudotime ordering of cells revealed 6 potential differentiation pathways of hemocytes.

(A) UMAP plot of scRNA-seq analysis showing the 7 transcriptomic clusters used for pseudotime analysis. 4 clusters were identified cytologically (SGC for small granule cells - cluster 3, H for hyalinocytes - cluster 2, ML for Macrophage Like - cluster 1 and VC for vesicular cells - cluster 7), cl.4, cl.5, and cl.6 represent clusters 4, 5, and 6, respectively. **(B)** Graphical representation (UMAP projection) of the Monocle 3 pseudo-time order of the clustered cells. Cluster 4 (cl.4) was used as the origin for the pseudotime analysis. **(C) (D) (E) (F) (G) and (H)** show the gene expression level of selected marker genes obtained from the monocle3 trajectory analysis at the beginning and end of the modelized differentiation pathways (in red on the UMAP plot) from cluster 4 to hyalinocytes, to Vesicular Cells (VC), to cluster 5 cells, to Macrophage-Like cells (ML), to cluster 6 cells, and to Small Granule Cells (SGC) respectively. The color scale represents the normalized expression level of each gene. **(I)** Dot plot showing the average expression and the percentage of cells expressing identified transcripts encoding for transcription factors in the scRNA-seq dataset. The scale represents the normalized expression level, while the dot diameter indicates the percentage of cells expressing the gene.

additional transcription factors were specifically identified in cluster 6 (CgGATA3, CgPU.1 and CgELF2), cluster 5 (CgELF2, CgELK3 and CgIRF1) and cluster 4 (CgTAL1 and CgFOS1). These data potentially define four distinct hematopoietic lineages originating from one type of immature blast cells and give rise to hyalinocytes, SGC (via VC and ML), or two distinct differentiated blast-like cells. We also identified a combination of transcription factors specific to lineages and cell types that are potential master regulators of cell fate during hematopoiesis.

Discussion

The findings of our study represent a significant advancement in our understanding of the functional diversity and lineages of *C. gigas* hemocytes. Single-cell RNA-seq and cytology were combined to identify seven distinct hemocyte transcriptomic cell clusters and an equivalent number of morphotypes. These include four granular cell types (big granule cells, macrophage-like cells, small granule cells and vesicular cells), two distinct blast-like cells (basophilic and acidophilic blast-like cells), and one agranular epithelial-like cell type (hyalinocytes). A significant challenge was to identify correlations between transcriptomic and cytological data to fully define each cytological cell type. This challenge was overcome by combining multiple approaches, including isopycnic Percoll density gradient fractionation combined with the analysis of transcriptomic markers expression, and functional assays including phagocytosis, oxidative burst, copper accumulation, AMP expression and finally pseudotime analysis of gene expression. These results confirmed the historical classification of the 3 main cell groups : blasts, hyalinocytes, and granular cells (15) and deepened our understanding of the functional specificities of poorly characterized cell types. In particular, we identified distinct transcriptional and functional subtypes among blasts and granular cells with complementary immune specialization and lineage relationships between cells.

One significant outcome of the present study is the identification of cell types involved in antimicrobial activities, including phagocytosis, intracellular copper accumulation, an oxidative burst and antimicrobial peptide production. These cell types have been extensively studied for their role in antibacterial and antiparasitic defenses, as they are found in the large majority of invertebrates (17). Nevertheless, there has been considerable debate surrounding the cell types specialized for these critical immune functions in bivalves, particularly oysters. Moreover, the involvement of the different hemocyte subpopulations in immune functions is not yet fully understood.

Our findings reveal that the macrophage-like (ML) cells and small granule cells (SGC) are the sole hemocyte cell types that function as professional phagocytes, as demonstrated against Zymosan or *Vibrio*. These two distinct cell types could be distinguished functionally. First, two distinct transcriptomic clusters were identified for each cell type (Cluster 1 for ML / BGC and Cluster 3 for SGC). Secondly, only ML induced a measurable oxidative burst. Thirdly, only SGC accumulated intracellular copper in specific granules. Interestingly, our scRNA-seq analysis indicates that SGC (cluster 3) expresses the scavenger receptor cysteine-rich (SRCR) gene G3876, annotated as an Low-density lipoprotein receptor-related protein with a Log2 fold change (Log2FC) of 0.77 linking them to scavenger receptor-mediated pathogen recognition and clearance. This aligns with findings by Wang et al. (43), who demonstrated significant expansion and dynamic regulation of SRCR genes in response to pathogen-associated molecular patterns. The pseudotime trajectory linking macrophage-like (ML) and small granule-like (SGC) cells suggests a potential developmental relationship within the granular cell lineage; however, this hypothesis requires further validation. The notion that ML could serve as a precursor for SGC may seem counterintuitive. However, this is not an isolated phenomenon among invertebrate hemocytes. For instance, in *Drosophila* larvae (44), some populations of professional phagocytes, the sessile plasmatocytes, give rise to crystal cells or lamellocytes that are morphologically and functionally distinct from plasmatocytes (45). Similarly, the existence of multiple professional phagocytes in the oyster is reminiscent of

vertebrate macrophages, polynuclear neutrophils and dendritic cells, which possess distinct functional specializations, including efferocytosis (46), oxidative burst, NETosis, or antigen presentation (47).

The characterization of professional phagocytes in oysters is of particular importance for a deeper understanding of oyster-*Vibrio* interactions during pathogenesis. Some of the most extensively studied oyster pathogens, including strains of *V. tasmaniensis* and *V. aestuarianus francensis,* harbor virulence traits that enable them to disrupt the phagocytic activity of hemocytes during pathogenesis. For instance, *V. tasmaniensis* behaves as a facultative intracellular pathogen with phagocytosis-dependent cytotoxicity (11). Additionally, both *V. tasmaniensis* and *V. aestuarianus* display resistance to copper toxicity through CopA and CusA/B transporters. This trait is essential for the survival and virulence of these pathogens in oysters (9, 48). Since SGCs have been demonstrated to be professional phagocytes with copper-rich granules, the cellular interactions between SGCs and these vibrios are likely to be critical during the antibacterial host response and pathogenesis. ML are phagocytes that possess a very potent NADPH-oxidase-dependent oxidative burst. The oxidative burst is a rapid and potent antimicrobial response observed in professional phagocytes, such as polynuclear neutrophils in mammals. It is worth noting that NADPH-dependent ETosis has been observed in *C. gigas* in a manner analogous to that observed in human neutrophils (49). This cell death is characterized by the projection of DNA extracellular traps that capture and kill some pathogens like *Vibrio* (49). Therefore, it is reasonable to hypothesize that ML may also be involved in ETosis.

The specialized functions of the two other types of granular cells, the BGCs and the VCs, remain unclear. Despite the difficulty in identifying a specific scRNAseq transcriptomic cluster for BGCs, the level of expression of laccase 24 was found to be higher in a particular subcluster among ML (Supp. Fig. S8) and pseudo-time analysis highlighted the same subcluster as an alternative differentiation state among ML (**Fig. 7B**). The enrichment of transcripts involved in oxido-reduction pathways, particularly laccase 24, aligns with their potential role in melanization and response to oxidative stress (50). While melanin-like deposits have been observed in some cases of infestation by the parasites *Martelia* or B*onamia* in the Sydney rock oyster (51), this mechanism is not as robust as that described in arthropods, which perform melanization through a prophenoloxidase activation cascade (52, 53). In many marine invertebrates (50), a type of hemocyte known as Brown Cells could be related to the BGCs described here. When observed without any staining (as in **Fig. 5F**), their big granules with a yellow to dark brown content appear to align with the historical description of brown cells that often infiltrate tissues (like gills) in animals exposed to polluted waters (50). It has therefore been theorized that these cells are involved in detoxification processes. Our pseudotime analysis indicates that they likely originate from ML, with limited phagocytosis activity and a specialized role in melanization and potentially heavy metal detoxification, as evidenced by rhodanine staining showing copper accumulation in some of their granules (**Fig. 5G**). Further studies are recommended to clarify the role of BGCs, particularly in the context of parasitic infestation or exposure to toxic stresses. Lastly, VC are granular cells that remain to be functionally characterized. Their transcriptomic profile suggests strong intracellular vesicular trafficking and autophagy activity. However, our functional assays did not reveal any particular immune-related function. Their clear granules appear auto-fluorescent when illuminated with UV light (**Supp. Fig. S12**) but the biochemical nature of the content of these granules remains to be characterized. As they also appear as cell intermediates along the granular cell differentiation pathway in pseudotime analysis, they could represent functionally immature precursors of the other three granular cell types, much like promyelocytes which possess specific azurophilic granules but are functionally immature precursors during granulocyte differentiation in humans. However, the enrichment of autophagy-related transcripts in VC calls for further investigation into a potential role in antiviral immunity, as autophagy has been suggested to play a role in the response to OsHV-1 virus (54).

Hyalinocytes are a homogenous cell type, with only one morphotype matching one transcriptomic cluster. It can be deduced from pseudotime analysis that they originate from a specific and very different differentiation pathway than the granular cells. According to the literature, hyalinocytes are involved in the early stages of inflammation and can infiltrate wounds and interact with foreign particles. In the flat oyster *Ostrea edulis*, they contribute to shell production and wound healing (55). In the Sydney rock oyster they play a role in cell aggregation (56), while in *C. virginica* (57) they contribute to encapsulation, reminiscent of lamellocytes in *Drosophila*. Our results suggest an important role of AMP expression in the immune response. Indeed, *Cg*-BigDefs, which participate in the control of oyster microbiota (58), were found to be expressed in both hyalinocytes and blast-like cells. Moreover, hyalinocytes from the oyster *O. edulis* have been shown to express the AMP Myticin C (59), which lends further support to this immune function. Among the AMPs, we also found that Cg-BPI and *Cg*-Defh, are more expressed in BBL, ABL than in other cell types. These results are somewhat unexpected, given the prevailing assumption that AMPs are stored in granules of granular cells, rather than agranular cells (16). These results highlight the necessity to reassess the role of specific agranular cell types in the active production of humoral immune effectors. Nevertheless, further staining approaches would be necessary to confirm these transcriptomic results. Our findings suggest that hyalinocytes and/or the blast-like cells may be a cellular target of the OsHV-1 virus, the causal agent of POMS, which dampens the expression of certain AMPs (7), thereby inducing bacterial dysbiosis. It is still unclear whether this is due to a decreased expression of AMPs and/or inhibition of immature blast cell differentiation involved in the renewal of agranular cell types.

It should be noted that the complexity of blast-like cells could not be fully elucidated in this study, as 3 clusters and only 2 morphotypes were identified. Cell fractionation using Percoll gradient failed to yield pure blast-enriched fractions (ABL and BBL), preventing precise functional characterization. The enrichment in transcripts of the transcription synthesis degradation continuum aligns with the definition of undifferentiated blast-type cells and with the basophilic staining obtained in MCDH for BBL cells, as immature blast cells are characterized by a basophilic cytoplasmic staining in humans. However, our results show that certain blast populations can produce AMPs, suggesting that these cells may also play a role in the production of humoral effectors. Ultimately, it remains unclear whether these circulating immature cells are indeed the stem cells from which all hemocytes originate.

In the animal kingdom, the innate immune system relies on specialized cells derived from pluripotent precursors through hematopoiesis. Transcription factors in particular have been found to exhibit a high degree of conservation throughout the animal kingdom, from invertebrates to vertebrates. However, the mechanisms underlying the functional differentiation of bivalves are only partially available or understood (60). Recent research has indicated the potential existence of hemocyte progenitors, also known as blast-like cells in several bivalve species. These include clams, mussels, scallops, marine mussels, freshwater mussels, oysters, pearl oysters, and wing shells (60). However, various models for hematopoiesis in bivalves have been proposed and extensively debated without a clear consensus or definitive proof. Single-cell RNA sequencing and pseudotime analysis have enabled us to propose a refined model of hematopoiesis at an unprecedented level of detail. In this model, the different types of hemocytes are likely produced through four differentiation pathways that originate from a common progenitor. One pathway results in the formation of agranular hyalinocytes, while another independent pathway gives rise to the granular cells, including VC, ML, BGC, and SGC. Furthermore, two additional differentiation pathways have been identified that may lead to terminally differentiated blast-like cells. The differentiation of mature hemocytes involves the establishment of lineage-specific gene expression profiles, which rely on transcription factors to modulate the expression of their target genes. Our study identified a combination of transcription factors that are differentially expressed during *C. gigas* hematopoiesis and are specific to differentiation stages and cell lineages, including many well-known hematopoietic transcription factors such as GATA, PU-1, TAL1 and SOX factors, which are positioned in this model of *C. gigas* hematopoiesis (61–63) (**Fig. 8**). Nevertheless,

we did not detect any canonical stem or progenitor cell populations in our dataset, underscoring the need for future investigations - potentially involving immunological challenges and lineage-tracing assays - to clarify whether proliferative cells circulate in the hemolymph or instead reside primarily in tissue compartments.

The comparison of hemocyte populations in *C. hongkongensis* and *C. gigas* highlights a shared reliance on granulocytes as primary immune effectors, with *C. hongkongensis* (27). Our study emphasizes functional specialization in *C. gigas*, focusing on phagocytosis, oxidative stress responses, and vesicular trafficking, likely reflecting differences in transcriptomic and functional characterization methodologies. Moreover, the identification of conserved transcription factors such as Tal1, Sox, Runx and GATA in both datasets underscores the evolutionary conservation of hematopoiesis pathways across metazoans. While direct comparisons between scRNA-seq datasets are hindered by differing annotation frameworks, parallels can still be drawn with studies in other invertebrates. For example, shrimp and crayfish scRNAseq datasets (64) describe hemocytes with immune-activated states and integrin-related markers, respectively, while *Anopheles gambiae* (65)exhibits clusters with high ribosomal activity and transcription factors such as bHLH and myc. These findings highlight both the shared molecular foundations and species-specific differences that define hemocyte diversity and specialization.

This study significantly advances our understanding of bivalve immunity, especially in comparison to arthropods. By introducing a standardized reference hemocytogram for oysters using MCDH staining, defining cell type-specific markers and key transcription factors likely involved in cell fate determination, as well as clarifying the functions of different hemocytes, we have paved the way for future in-depth studies. Moreover, the identified clusters represent functionally and transcriptionally distinct cell populations under the conditions studied, yet they may reflect dynamic states rather than fixed subtypes, thereby acknowledging the potential for hemocyte populations to transition between states in response to environmental or physiological changes—even under homeostatic conditions. This will facilitate further studies of the oyster's immune response to various biotic and abiotic stress at the cellular level. Improved comprehension of antiviral and antibacterial responses in bivalves, along with an enhanced understanding of immune priming and immune memory at the cellular level in bivalves, will benefit health and population management practices for sustainable aquaculture production. These findings will also contribute to the broader field of evolutionary immunology by enabling comparative studies and elucidating the diversification of immune cells and immunity-related genes in a protostome.

Materials and methods

Conservation of oysters

The work described here was performed using two different sources of oysters of the same species *Crassostrea (Magallana) gigas*. ISA (Ifremer Standardized Oysters - La tremblade - France) oysters for the scRNA-seq experiment and oysters provided by a local supplier (*https://www.huitres-bouzigues.com*). Animals were washed and kept in 10 L tanks containing seawater and a bubbler to oxygenate and homogenize the water. Water was changed daily and oyster health was monitored. All animals used in this study were 18 months of age.

Hemocyte collection and processing

Crassostrea gigas hemocytes were collected from live animals by puncture of the adductor muscle. The oyster shell was incised on the posterior side with forceps. Hemolymph was collected using a 23Gx1" needle mounted on a 5 mL syringe prefilled with 2 mL of ice-cold Alsever modified medium (20.8 g glucose – 8 g trisodium citrate - 22.5 g sodium chloride - 0.4 g BSA - pH=7.5). Samples were centrifuged for 4 minutes at 200 g – 4 °C and the supernatant was removed and

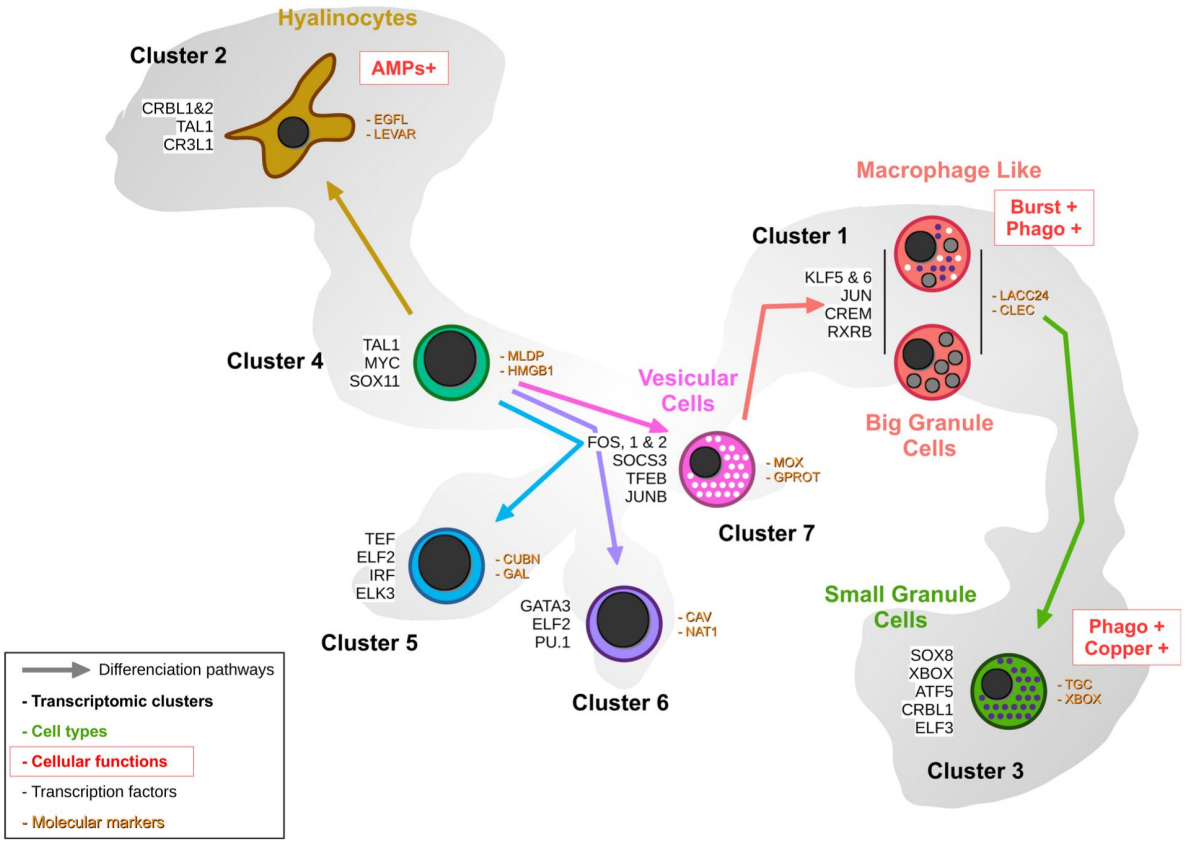

Figure 8.

Proposed hemocyte ontology in *Crassostrea gigas* based on the transcriptomic, cytological and functional results obtained.

Cells are colored according to the same color code as the transcriptomic clusters. Cluster numbers and cell types are indicated. To the left of the cells are the overexpressed transcription factors and to the right are the identified marker genes in each cluster. Functional characteristics of hyalinocytes, macrophage-like cells and small granule cells are marked in red. (**AMP** : AntiMicrobial Peptide, **Burst** : ROS production, **Phago** : phagocytosis)

replaced with 1 mL of fresh Alsever modified medium. Each hemocyte sample was thoroughly checked for quality, counted under a microscope using KOVA (Kova International, USA) slides, and stored on ice prior to processing. For scRNA-seq analysis, resuspended hemocytes were filtered on 30 µm filters, counted, the solution was adjusted to 1.10^6 cells per mL and stored on ice prior to 10X genomic library preparation.

C. gigas genome annotation

The *C. gigas* genome (Genbank GCA_902806645.1) (30) was used as a reference. Prior to annotation, the longest CDS sequences were extracted from the gff3 file. Annotation was realized using the ORSON script (*https://gitlab.ifremer.fr/bioinfo/workflows/orson*). ORSON combines cutting-edge tools for annotation processes within a Nextflow pipeline. The ORSON script performs a sequence similarity search with BLAST (66) against the Uniprot-Swissprot and Uniprot-trEMBL databases, and functional prediction with InterProScan (67) and eggNOG (68) orthogroup annotation. Interproscan analysis was performed against Pfam, Prosite, CDD, TIGR, SMART, SuperFamily, PRINTS and Hamap databases. Results were collected and processed using Blast2GO (69) for annotation mapping and validation.

Drop Seq-based scRNA-seq library generation

The 10X Genomics protocol, Single Cell 3' Reagent Kits v2 User Guide from the manufacturer (10X Genomics, USA) was followed to prepare gel in emulsion beads (GEM) containing single cells, hydrogel beads, and reverse transcription reagents, perform barcoded cDNA synthesis, and generate sequencing libraries from pooled cDNAs. The concentration of single-cell suspensions was approximately 1000 cells / µL, as estimated by manual counting, and cells were loaded according to the 10X protocol to capture approximately 3000 cells per reaction. Library construction (after GEM digestion) was performed using 10X reagents according to the manufacturer's instructions. Libraries (paired-end reads 75 bp) were sequenced on an Illumina NovaSeq (Illumina, USA) using two sequencing lanes per sample.

scRNA-seq analysis

Reads were aligned to the *C. gigas* reference genome (Genbank GCA_902806645.1) (27) using STAR solo software (v 2.7.10) (29). Unique molecular identifiers (UMIs) were extracted and counted for each cell, and an expression matrix was generated for further analysis. Single-cell RNA sequencing (scRNA-seq) data analysis was performed using the R programming language (version 4.2.1) (R Core Team, 2018) and the Seurat package (version 4.3.0) (70). The data were then pre-processed to remove unwanted sources of variation and to normalize gene expression. Cells with small library sizes and a high proportion of mitochondrial genes were excluded. Data normalization was performed using the SCTransform method. After normalization, highly variable genes were identified using the FindVariableFeatures function and the top variable genes were selected for downstream analyses. Dimensionality reduction was performed using Principal Component Analysis (PCA), followed by Uniform Manifold Approximation and Projection (UMAP) to visualize the data. Cell clustering was performed using the 'FindClusters' function, using the previously identified significant principal components (dims = 6) and a resolution parameter (r = 0.1) to define cluster granularity. Differential expression analysis was performed using the 'FindAllMarkers' function (pct.min = 0.25) to identify genes differentially expressed between clusters, with statistical significance determined using the Wilcoxon rank sum test. Functional enrichment analysis of differentially expressed genes was performed using gene set enrichment analysis (RBGOA) (33).

KEGG pathway analysis

KEGG analysis was performed using DAVID Bioinformatics Resources (NIAID/NIH) (32). Gene lists of specifically overexpressed genes in each cluster were obtained after scRNA-seq processing (genes with Log2FC > 0.25 and significant p-value < 0.001) and used for KEGG annotation. The *C.*

gigas reference genome from the DAVID bioinformatics resource was used for this analysis, with thresholds of 2 for counts and 0.05 for EASE value (p-value). KEGG annotation results were post-processed and presented as a heatmap showing the KEGG pathway, fold enrichment, p-value significance and number of positive terms.

Rank-Based Gene Ontology Analysis

RBGOA first clusters GOs according to their representative genes to identify the most significant GOs, and then ranks the identified biological processes according to their average expression levels (over all representative genes). Finally, biological processes, molecular functions and cellular components significantly enriched in DEGs are identified by a Mann-Whitney rank test with a strict FDR correction. The files generated by the GO-MWU scripts (*https://github.com/z0on/GO_MWU*) were post-processed to extract the category names and the fraction indicating the number of "good candidates" relative to the total number of genes belonging to that category. The "good candidates" were the genes that exceeded an arbitrary 'absValue' cutoff (defined as 0.001) in their significance measure. The results were presented as a heatmap.

Percoll Density Gradient Separation of Hemocytes10.3390/cells13242106

A concentration series of Percoll (Cytiva, Sweden) diluted in Alsever modified medium was prepared as follows: 10, 20, 30, 40, 50, 60 and 70 % (vol/vol). Discontinuous density gradients (from 10 % Percoll with a density of 1.0647 to 70 % Percoll with d=1.1049) were made using 1.5 mL of each concentration and loaded with 1 mL of the hemocyte suspension corresponding to approximately 2.10^7 cells. Centrifugation was performed (30 min, 800 g, 4 °C) in a swinging bucket on a Beckman Coulter JS-13.1 rotor (Beckman Coulter, USA). Hemocytes concentrated at each density interface were collected separately with a 70 mm long 20Gx2.75" needle mounted on a 1 mL syringe. The hemocytes were then washed from the Percoll by adding 10 mL of ice-cold Alsever modified medium, pelleted by centrifugation (10 min, 200 g, 4°C) and resuspended in Alsever modified medium or filtered seawater.

Cytological description of the hemocyte populations

200,000 fresh hemocytes were seeded onto a slide using a Cytospin 4 centrifuge (Thermo Scientific, USA). The samples were then stained using the panoptic MCDH (Micro Chromatic Detection for Hematology) (Cellavision, Sweden) staining protocol. This protocol produces purple hues typical of Romanowsky-Giemsa staining results. After staining, the samples were observed using a LEICA DMR (Leica AG, Germany) transmitted light microscope with a 40x magnification objective. Each slide was imaged and the hemocytes were counted and characterized based on their morphology.

Real Time-quantitative Polymerase Chain Reaction (RT-qPCR)

Total RNA was extracted using the RNeasy kit (Qiagen, the Netherlands) and cDNA was synthesized from 1 µg total RNA using the Superscript IV kit (ThermoFisher Scientific, USA) with oligo(dT) primers. RT-PCR was performed on LightCycler© 480 thermocycler using the SYBR Green 1 Master kit (Roche, Switzerland). Primers were used at 200 nM. Primer sequences are listed in *Supplementary Table S3*. Expression was normalized to *Cg-rps6* reference gene. The standard cycling conditions were 95°C pre-incubation for 3 minutes followed by 40 cycles of 95°C for 10 seconds, 60°C for 20 seconds, and 72°C for 25 seconds. Each pair of primers was first tested and validated on a total hemocyte RNA preparation to control melting curves and establish calibration lines.

Oxidative Burst Assay

The production of reactive oxygen species was quantified by luminescence assay. Briefly, hemocytes from hemolymph puncture or Percoll density gradient were washed once with filtered sterile water. 50 µL of hemocytes were plated in triplicate on a 96-well plate (3.10^5 cells/cm²). 50 µL of 40 mM luminol (Merck and Co, USA) was added to each well. After 45 minutes of incubation at room temperature, the oxidative burst was induced by adding 100 µL of zymosan (Merck and Co, USA) at a multiplicity of infection (MOI) of 50:1. The plate was immediately placed in a Berthold Centro XS3 LB 960 luminescence microplate reader (Berthold GmbH, Germany) to measure luminescence emission every 2 minutes for 2 hours.

Phagocytosis assay

400 µL of filtered, sterile water-washed hemocytes were seeded in a 24-well plate at a concentration of 3.10^5 cells/cm². After 15 minutes, 50 µL of zymosan was added to the fractions at an MOI of 20:1. For LMG20012^T Vibrio, 50 µL of bacteria was added to a total hemolymph at an MOI of 5:1. After 1 hour of contact at room temperature, the cells were resuspended and 200 µL of the suspension was applied to a microscope slide using a Cytospin centrifuge. The slides were then stained with MCDH and observed under a LEICA DMR transmitted light microscope with a 40x magnification objective (Leica AG, Germany) to count phagocytic cells. A total of 2,807 cells were examined in three independent experiments.

NitroBlueTetrazolium (NBT) staining

ROS production was measured using NitroBlue Tetrazolium reduction after zymosan stimulation. Briefly, 1 mL (1.10^6 cells) of hemocyte solution was mixed with 50 µL of filtered NBT solution (15 mg/mL in water). Zymosan was added at a 4:1 MOI and the mixture was incubated at room temperature for 10 minutes on a rocking shaker. Then, 50 µL of each sample was plated onto glass coverslips and observed under a transmitted light microscope LEICA DMR with a 40x magnification objective (Leica AG, Germany) to count NBT-positive cells. The positions of positive NBT cells were recorded prior to MCDH staining to identify hemocyte types.

Rhodanine copper staining of hemocytes

The storage of copper by hemocytes was examined by Rhodanine staining. Briefly, 1.10^5 hemocytes were plated on Superfrost slides using a cytospin and circled with a hydrophobic pen to retain the staining solution. The Copper Stain Kit (SkyTek, USA) was used to stain the hemocytes. As described by the kit manufacturer, one drop of Rhodanine solution was added to 9 drops of acetate to form the working solution. Five drops were placed on the cytospin cells and a 5 mL Eppendorf tube with the cap removed was placed over the cells to prevent evaporation of the working solution. The slide and the balanced Eppendorf tube were placed in a beaker of boiling distilled water for 20 minutes. The slide was then washed with 5 drops of acetate and 3 drops of hematoxylin were placed on the slide for 1 minute at room temperature. The slides were then washed a final time with acetate and observed under a LEICA DMR transmitted light microscope with a 40x magnification objective (Leica AG, Germany) to count rhodanine-positive cells. The positions of rhodanine-positive cells were recorded prior to MCDH staining to identify hemocyte types.

Pseudotemporal ordering of cells with Monocle3

Cells from the *C. gigas* dataset were analyzed using Monocle3 (*https://github.com/cole-trapnell-lab/monocle3*) (42). The Monocle3 analysis was performed on the Seurat object following the aforementioned processing steps. Clustering information (features, genes, partitions, clusters and UMAP coordinates) was transferred to a CDS object. The cell trajectory was calculated using the *learn_graph* function. The *choose_graph_segments* function was used to select three lineages. The

gene expression along pseudotime data was extracted from the result. Then, the data were used to plot genes along pseudotime in three lineages using ggplot2 v3.4.4 R package and the heatmap was generated using the pheatmap v1.0.12 R package.

Statistical Analysis

To evaluate differences between samples, a statistical analysis was performed using (version 4.2.1) (R Core Team, 2018) and appropriate packages. All data were examined for normality, and statistical tests were selected accordingly. One-way analysis of variance (ANOVA) was used for normally distributed data. Seven different hemolymph samples were used for cytological analysis. Oysters were provided by our local supplier and approximately 300 hemocytes were counted per sample. Seven independent experiments were performed for Percoll density gradient separation. A Tukey test was used to evaluate the statistical difference between the proportions of hemocyte types. The phagocytic capacity of hemocytes was tested in three independent experiments and statistical differences were evaluated using the Tukey test for both the phagocytic capacity between hemocyte types and the number of particles per phagocyte. Finally, oxidative burst capacity was tested 3 times on Percoll-separated hemocytes. The Tukey test was also used to assess statistical differences between conditions. The null hypothesis was rejected at a significance level of $p = 0.05$.

Data and materials availability

All data needed to evaluate the conclusions in the paper are present in the paper and/or the Supplementary Materials. Raw reads are available at ENA under the project accession number PRJEB74031.

Acknowledgements

We are grateful to the staff of the Ifremer platform of “La Tremblade” for technical support in animal housing. scRNA-seq data generated and used in this work were produced through the MGX platform (University of Montpellier, CNRS,INSERM). We thank the bioinformatic service of Ifremer (SEBIMER) for their help in bioinformatics and the qPCR platform GenSeq (University of Montpellier). We would like to thank Viviane Boulo and Danielle Mello for their enriching discussions, as well as all the members of the 2MAP laboratory team for the fruitful discussions throughout this project.

Additional information

Ethics

This work did not require ethical approval from a human subject or animal welfare committee.

Funding

This work was funded by the Agence Nationale de la Recherche (MOSAR-DEF, ANR-19-CE18-0025; DECICOMP, ANR-19-CE20-0004 and TRANSCAN ANR-18-CE35-0009), the University of Montpellier, iSite MUSE and the “GT-Huître” initiative from Ifremer. This study falls within the framework of the “Laboratoires d’Excellence (LABEX)” Tulip (ANR-10-LABX-41). Sébastien De La Forest Divonne was awarded a PhD grant from the Region Occitanie (HemoFight project) and the University of Perpignan Via Domitia graduate school ED305.

Author contributions

Conceptualization: G.M., D.D.-G., B.G., G.M.C. and E.V.

Methodology: S.d.L.F.D., J.P., G.M., D.D.-G., B.G., G.M.C. and E.V.

Investigation: S.d.L.F.D., J.P., G.M.C. and E.V. Supervision: G.M.C. and E.V.

Writing (original draft): S.d.L.F.D. and E.V.

Writing (review and editing): all authors.

Declaration of AI use

We have not used AI-assisted technologies in creating this article.

Additional files

Supplemental figures and tables

Supplemental Data S1

Supplemental Data S2

Supplemental Data S3

References

1. Bar-On Y. M., Phillips R., Milo R. (2018) **The biomass distribution on Earth** *Proceedings of the National Academy of Sciences* **115**:6506–6511

2. Leicester Bayne B. (2017) **Biology of Oysters** Academic Press

3. Zhang G., Li L., Meng J., Qi H., Qu T., Xu F., Zhang L. (2016) **Molecular Basis for Adaptation of Oysters to Stressful Marine Intertidal Environments** *Annu. Rev. Anim. Biosci* **4**:357–381

4. FAO (2023) **Global aquaculture production** *Fisheries and aquaculture division*

5. Pernet F., Lupo C., Bacher C., Whittington R. J. (2016) **Infectious diseases in oyster aquaculture require a new integrated approach** *Philosophical Transactions of the Royal Society B: Biological Sciences* **371**

6. Alfjorden A., Areskog M., Bruno D., Carnegie R., Cheslett D., Feist S., Ford S., Jones S., Lillehaug A., Madsen L., Renault T., Ruane N., Vennerstrom P. (2017) **New Trends in Important Diseases Affecting the Culture of Fish and Molluscs in the ICES Area 2002– 2015** *ICES cooperative research report* https://doi.org/10.17895/ices.pub.2800

7. de Lorgeril J., Lucasson A., Petton B., Toulza E., Montagnani C., Clerissi C., Vidal-Dupiol J., Chaparro C., Galinier R., Escoubas J.-M., Haffner P., Dégremont L., Charrière G. M., Lafont M., Delort A., Vergnes A., Chiarello M., Faury N., Rubio T., Leroy M. A., Pérignon A., Régler D., Morga B., Alunno-Bruscia M., Boudry P., Le Roux F., Destoumieux-Garzón D., Gueguen Y, Mitta G (2018) **Immune-suppression by OsHV-1 viral infection causes fatal bacteraemia in Pacific oysters** *Nat Commun* **9**:4215

8. Coyle N. M., O'Toole C., Thomas J. C. L., Ryder D., Feil E. J., Geary M., Bean T. P., Joseph A. W., Waine A., Cheslett D., Verner-Jeffreys D. W. (2023) **Vibrio aestuarianus clade A and clade B isolates are associated with Pacific oyster (Magallana gigas) disease outbreaks across Ireland** *Microbial Genomics* **9**

9. Mesnil A., Jacquot M., Garcia C., Tourbiez D., Canier L., Bidois A., Dégremont L., Cheslett D., Geary M., Vetri A., Roque A., Furones D., Garden A., Orozova P., Arzul I., Sicard M., Charrière G. M., Destoumieux-Garzón D., Travers M.-A. (2023) **Emergence and clonal expansion of Vibrio aestuarianus lineages pathogenic for oysters in Europe** *Molecular Ecology* **32**:2869–2883

10. Oyanedel D., Lagorce A., Bruto M., Haffner P., Morot A., Labreuche Y., Dorant Y., de La Forest Divonne S., Delavat F., Inguimbert N., Montagnani C., Morga B., Toulza E., Chaparro C., Escoubas J.-M., Gueguen Y., Vidal-Dupiol J., de Lorgeril J., Petton B., Degremont L., Tourbiez D., Pimparé L.-L., Leroy M., Romatif O., Pouzadoux J., Mitta G., Le Roux F., Charrière G. M., Travers M.-A., Destoumieux-Garzón D. (2023) **Cooperation and cheating orchestrate Vibrio assemblages and polymicrobial synergy in oysters infected with OsHV-1 virus** *Proceedings of the National Academy of Sciences* **120**:e2305195120

11. Rubio T., Oyanedel D., Labreuche Y., Toulza E., Luo X., Bruto M., Chaparro C., Torres M., de Lorgeril J., Haffner P., Vidal-Dupiol J., Lagorce A., Petton B., Mitta G., Jacq A., Le Roux F., Charrière G. M., Destoumieux-Garzón D. (2019) **Species-specific mechanisms of cytotoxicity**

toward immune cells determine the successful outcome of Vibrio infections *Proceedings of the National Academy of Sciences* **116**:14238–14247

12. Labreuche Y., Le Roux F., Henry J., Zatylny C., Huvet A., Lambert C., Soudant P., Mazel D., Nicolas J.-L. (2010) **Vibrio aestuarianus zinc metalloprotease causes lethality in the Pacific oyster Crassostrea gigas and impairs the host cellular immune defenses** *Fish Shellfish Immunol* **29**:753–758

13. Lafont M., Vergnes A., Vidal-Dupiol J., de Lorgeril J., Gueguen Y., Haffner P., Petton B., Chaparro C., Barrachina C., Destoumieux-Garzon D., Mitta G., Gourbal B., Montagnani C. (2020) **A Sustained Immune Response Supports Long-Term Antiviral Immune Priming in the Pacific Oyster, Crassostrea gigas** *mBio* **11** https://doi.org/10.1128/mbio.02777-19

14. Fallet M., Montagnani C., Petton B., Dantan L., de Lorgeril J., Comarmond S., Chaparro C., Toulza E., Boitard S., Escoubas J.-M., Vergnes A., Le Grand J., Bulla I., Gueguen Y., Vidal-Dupiol J., Grunau C., Mitta G., Cosseau C. (2022) **Early life microbial exposures shape the Crassostrea gigas immune system for lifelong and intergenerational disease protection** *Microbiome* **10**

15. de la Ballina N. R., Maresca F., Cao A., Villalba A. (2022) **Bivalve Haemocyte Subpopulations: A Review** *Front. Immunol* **13**

16. Bachère E., Rosa R. D., Schmitt P., Poirier A. C., Merou N., Charrière G. M., Destoumieux-Garzón D. (2015) **The new insights into the oyster antimicrobial defense: Cellular, molecular and genetic view** *Fish & Shellfish Immunology* **46**:50–64

17. Escoubas J.-M., Gourbal B., Duval D., Green T. J., Charrière G. M., Destoumieux-Garzón D., Montagnani C. (2016) **Immunity in Molluscs** In: Ratcliffe M. J. H., editors. *Encyclopedia of Immunobiology* Academic Press, Oxford pp. 417–436 https://www.sciencedirect.com/science/article/pii/B9780123742797120041

18. Mount A. S., Wheeler A. P., Paradkar R. P., Snider D. (2004) **Hemocyte-Mediated Shell Mineralization in the Eastern Oyster** *Science* **304**:297–300

19. Fischer W. S. S. (1988) **Environmental influence on bivalve hemocyte function** *Am Fish Soc Symp* **18**:225–237

20. Donaghy L., Hong H.-K., Lee H.-J., Jun J.-C., Park Y.-J., Choi K.-S. (2010) **Hemocyte parameters of the Pacific oyster Crassostrea gigas a year after the Hebei Spirit oil spill off the west coast of Korea** *Helgol Mar Res* **64**:349–355

21. de la Ballina N. R., Villalba A., Cao A. (2020) **Differences in proteomic profile between two haemocyte types, granulocytes and hyalinocytes, of the flat oyster Ostrea edulis** *Fish & Shellfish Immunology* **100**:456–466

22. Wang W., Li M., Wang L., Chen H., Liu Z., Jia Z., Qiu L., Song L. (2017) **The granulocytes are the main immunocompetent hemocytes in Crassostrea gigas** *Developmental & Comparative Immunology* **67**:221–228

23. Mao F., Wong N.-K., Lin Y., Zhang X., Liu K., Huang M., Xu D., Xiang Z., Li J., Zhang Y., Yu Z. (2020) **Transcriptomic Evidence Reveals the Molecular Basis for Functional Differentiation of Hemocytes in a Marine Invertebrate, Crassostrea gigas** *Front. Immunol* **11**

24. Zhang H., Wang H., Chen H., Wang M., Zhou Z., Qiu L., Wang L., Song L. (2019) **The transcriptional response of the Pacific oyster Crassostrea gigas under simultaneous**

bacterial and heat stresses *Developmental & Comparative Immunology* **94**:1–10

25. Zhang E., Li Z., Dong L., Feng Y., Sun G., Xu X., Wang Z., Cui C., Wang W., Yang J. (2024) **Exploration of Molecular Mechanisms of Immunity in the Pacific Oyster (Crassostrea gigas) in Response to Vibrio alginolyticus Invasion** *Animals* **14**:1707

26. Nguyen T. V., Alfaro A. C., Merien F. (2019) **Omics approaches to investigate host–pathogen interactions in mass mortality outbreaks of Crassostrea gigas** *Reviews in Aquaculture* **11**:1308–1324

27. Meng J., Zhang G., Wang W.-X. (2022) **Functional heterogeneity of immune defenses in molluscan oysters Crassostrea hongkongensis revealed by high-throughput single-cell transcriptome** *Fish & Shellfish Immunology* **120**:202–213

28. Rosa R. D., Alonso P., Santini A., Vergnes A., Bachère E. (2015) **High polymorphism in big defensin gene expression reveals presence–absence gene variability (PAV) in the oyster Crassostrea gigas** *Developmental & Comparative Immunology* **49**:231–238

29. Kaminow B., Yunusov D., Dobin A. (2021) **STARsolo: accurate, fast and versatile mapping/quantification of single-cell and single-nucleus RNA-seq data** *bioRxiv* https://doi.org/10.1101/2021.05.05.442755

30. Peñaloza C., Gutierrez A. P., Eöry L., Wang S., Guo X., Archibald A. L., Bean T. P., Houston R. D. (2021) **A chromosome-level genome assembly for the Pacific oyster Crassostrea gigas** *GigaScience* **10**:giab020

31. Satija R., Farrell J. A., Gennert D., Schier A. F., Regev A. (2015) **Spatial reconstruction of single-cell gene expression data** *Nat Biotechnol* **33**:495–502

32. Sherman B. T., Hao M., Qiu J., Jiao X., Baseler M. W., Lane H. C., Imamichi T., Chang W. (2022) **DAVID: a web server for functional enrichment analysis and functional annotation of gene lists (2021 update)** *Nucleic Acids Research* **50**:W216–W221

33. Wright R. M., Aglyamova G. V., Meyer E., Matz M. V. (2015) **Gene expression associated with white syndromes in a reef building coral, Acropora hyacinthus** *BMC Genomics* **16**

34. Bachère E., Chagot D., Grizel H. (1988) **Separation of Crassostrea gigas hemocytes by density gradient centrifugation and counterflow centrifugal elutriation** *Developmental & Comparative Immunology* **12**:549–559

35. Lambert C., Soudant P., Choquet G., Paillard C. (2003) **Measurement of Crassostrea gigas hemocyte oxidative metabolism by flow cytometry and the inhibiting capacity of pathogenic vibrios** *Fish & Shellfish Immunology* **15**:225–240

36. Schmitt P., Rosa R., Duperthuy M., de Lorgeril J., Bachère E., Destoumieux-Garzon D. (2012) **The Antimicrobial Defense of the Pacific Oyster, Crassostrea gigas. How Diversity may Compensate for Scarcity in the Regulation of Resident/Pathogenic Microflora** . *Frontiers in Microbiology* **3**

37. Vogt G. (2012) **Hidden Treasures in Stem Cells of Indeterminately Growing Bilaterian Invertebrates** *Stem Cell Rev and Rep* **8**:305–317

38. Jemaà M., Morin N., Cavelier P., Cau J., Strub J. M., Delsert C. (2014) **Adult somatic progenitor cells and hematopoiesis in oysters** *Journal of Experimental Biology* **217**:3067–3077

39. Fahl S. P., Wang M., Zhang Y., Duc A.-C. E., Wiest D. L. (2015) **Regulatory Roles of Rpl22 in Hematopoiesis: An Old Dog with New Tricks** *Crit Rev Immunol* **35**:379–400

40. Rehn M., Wenzel A., Frank A.-K., Schuster M. B., Pundhir S., Jørgensen N., Vitting-Seerup K., Ge Y., Jendholm J., Michaut M., Schoof E. M., Jensen T. L., Rapin N., Sapio R. T., Andersen K. L., Lund A. H., Solimena M., Holzenberger M., Pestov D. G., Porse B. T. (2022) **PTBP1 promotes hematopoietic stem cell maintenance and red blood cell development by ensuring sufficient availability of ribosomal constituents** *Cell Reports* **39**

41. Athanasiadis E. I., Botthof J. G., Andres H., Ferreira L., Lio P., Cvejic A. (2017) **Single-cell RNA-sequencing uncovers transcriptional states and fate decisions in haematopoiesis** *Nat Commun* **8**:2045

42. Cao J., Spielmann M., Qiu X., Huang X., Ibrahim D. M., Hill A. J., Zhang F., Mundlos S., Christiansen L., Steemers F. J., Trapnell C., Shendure J. (2019) **The single-cell transcriptional landscape of mammalian organogenesis** *Nature* **566**:496–502

43. Wang L., Zhang H., Wang M., Zhou Z., Wang W., Liu R., Huang M., Yang C., Qiu L., Song L. (2019) **The transcriptomic expression of pattern recognition receptors: Insight into molecular recognition of various invading pathogens in Oyster Crassostrea gigas** *Developmental & Comparative Immunology* **91**:1–7

44. Hultmark D., Andó I. (2022) **Hematopoietic plasticity mapped in Drosophila and other insects** *eLife* **11**:e78906

45. Banerjee U., Girard J. R., Goins L. M., Spratford C. M. (2019) **Drosophila as a Genetic Model for Hematopoiesis** *Genetics* **211**:367–417

46. Boada-Romero E., Martinez J., Heckmann B. L., Green D. R. (2020) **The clearance of dead cells by efferocytosis** *Nat Rev Mol Cell Biol* **21**:398–414

47. Dale D. C., Boxer L., Liles W. C. (2008) **The phagocytes: neutrophils and monocytes** *Blood* **112**:935–945

48. Vanhove A. S., Rubio T. P., Nguyen A. N., Lemire A., Roche D., Nicod J., Vergnes A., Poirier A. C., Disconzi E., Bachère E., Le Roux F., Jacq A., Charrière G. M., Destoumieux-Garzón D. (2016) **Copper homeostasis at the host vibrio interface: lessons from intracellular vibrio transcriptomics** *Environmental Microbiology* **18**:875–888

49. Poirier A. C., Schmitt P., Rosa R. D., Vanhove A. S., Kieffer-Jaquinod S., Rubio T. P., Charrière G. M., Destoumieux-Garzón D. (2014) **Antimicrobial Histones and DNA Traps in Invertebrate Immunity: Evidences in Crassostrea Gigas *** *Journal of Biological Chemistry* **289**:24821–24831

50. Zaroogian G., Yevich P. (1993) **Cytology and biochemistry of brown cells in Crassostrea virginica collected at clean and contaminated stations** *Environmental Pollution* **79**:191–197

51. Allam B., Raftos D. (2015) **Immune responses to infectious diseases in bivalves** *Journal of Invertebrate Pathology* **131**:121–136

52. Nakhleh J., El Moussawi L., Osta M. A. (2017) **Chapter Three - The Melanization Response in Insect Immunity** In: Ligoxygakis P., editors. *Advances in Insect Physiology* Academic Press pp. 83–109

53. Amparyup P., Charoensapsri W., Tassanakajon A. (2013) **Prophenoloxidase system and its role in shrimp immune responses against major pathogens** *Fish & Shellfish Immunology* **34**:990–1001

54. Picot S., Faury N., Pelletier C., Arzul I., Chollet B., Dégremont L., Renault T., Morga B. (2022) **Monitoring Autophagy at Cellular and Molecular Level in Crassostrea gigas During an Experimental Ostreid Herpesvirus 1 (OsHV-1) Infection** *Front. Cell. Infect. Microbiol* **12**

55. de la Ballina N. R., Villalba A., Cao A. (2020) **Differences in proteomic profile between two haemocyte types, granulocytes and hyalinocytes, of the flat oyster Ostrea edulis** *Fish & Shellfish Immunology* **100**:456–466

56. Aladaileh S., Nair S. V., Birch D., Raftos D. A. (2007) **Sydney rock oyster (Saccostrea glomerata) hemocytes: Morphology and function** *Journal of Invertebrate Pathology* **96**:48–63

57. Rifkin E., Cheng T. C., Hohl H. R. (1969) **An electron-microscope study of the constituents of encapsulating cysts in the American oyster, Crassostrea virginica, formed in response to Tylocephalum metacestodes** *Journal of Invertebrate Pathology* **14**:211–226

58. De San Nicolas N., Asokan A., Rosa R. D., Voisin S. N., Travers M.-A., Rocha G., Dantan L., Dorant Y., Mitta G., Petton B., Charrière G. M., Escoubas J.-M., Boulo V., Pouzadoux J., Meudal H., Loth K., Aucagne V., Delmas A. F., Bulet P., Montagnani C., Destoumieux-Garzón D. (2022) **Functional Diversification of Oyster Big Defensins Generates Antimicrobial Specificity and Synergy against Members of the Microbiota** *Marine Drugs* **20**

59. de la Ballina N. R., Villalba A., Cao A. (2021) **Shotgun analysis to identify differences in protein expression between granulocytes and hyalinocytes of the European flat oyster Ostrea edulis** *Fish Shellfish Immunol* **119**:678–691

60. Pila E. A., Sullivan J. T., Wu X. Z., Fang J., Rudko S. P., Gordy M. A., Hanington P. C. (2016) **Haematopoiesis in molluscs: A review of haemocyte development and function in gastropods, cephalopods and bivalves** *Developmental & Comparative Immunology* **58**:119–128

61. de Bruijn M., Dzierzak E. (2017) **Runx transcription factors in the development and function of the definitive hematopoietic system** *Blood* **129**:2061–2069

62. Scott E. W., Simon M. C., Anastasi J., Singh H. (1994) **Requirement of transcription factor PU.1 in the development of multiple hematopoietic lineages** *Science* **265**:1573–1577

63. Bergiers I., Andrews T., Vargel Bölükbaşı Ö., Buness A., Janosz E., Lopez-Anguita N., Ganter K., Kosim K., Celen C., Itır Perçin G., Collier P., Baying B., Benes V., Hemberg M., Lancrin C. (2018) **Single-cell transcriptomics reveals a new dynamical function of transcription factors during embryonic hematopoiesis** *eLife* **7**:e29312

64. Xin F., Zhang X. (2023) **Hallmarks of crustacean immune hemocytes at single-cell resolution** *Front. Immunol* **14**

65. Kwon H., Mohammed M., Franzén O., Ankarklev J., Smith R. C. (2021) **Single-cell analysis of mosquito hemocytes identifies signatures of immune cell subtypes and cell differentiation** *eLife* **10**:e66192

66. Altschul S. F., Gish W., Miller W., Myers E. W., Lipman D. J. (1990) **Basic local alignment search tool** *Journal of Molecular Biology* **215**:403–410

67. Jones P., Binns D., Chang H.-Y., Fraser M., Li W., McAnulla C., McWilliam H., Maslen J., Mitchell A., Nuka G., Pesseat S., Quinn A. F., Sangrador-Vegas A., Scheremetjew M., Yong S.-Y., Lopez R., Hunter S. (2014) **InterProScan 5: genome-scale protein function classification** *Bioinformatics* **30**:1236–1240

68. Cantalapiedra C. P., Hernández-Plaza A., Letunic I., Bork P., Huerta-Cepas J. (2021) **eggNOG-mapper v2: Functional Annotation, Orthology Assignments, and Domain Prediction at the Metagenomic Scale** *Molecular Biology and Evolution* **38**:5825–5829

69. Götz S., García-Gómez J. M., Terol J., Williams T. D., Nagaraj S. H., Nueda M. J., Robles M., Talón M., Dopazo J., Conesa A. (2008) **High-throughput functional annotation and data mining with the Blast2GO suite** *Nucleic Acids Research* **36**:3420–3435

70. Hao Y., Hao S., Andersen-Nissen E., Mauck W. M., Zheng S., Butler A., Lee M. J., Wilk A. J., Darby C., Zager M., Hoffman P., Stoeckius M., Papalexi E., Mimitou E. P., Jain J., Srivastava A., Stuart T., Fleming L. M., Yeung B., Rogers A. J., McElrath J. M., Blish C. A., Gottardo R., Smibert P., Satija R. (2021) **Integrated analysis of multimodal single-cell data** *Cell* **184**:3573–3587

Author information

Sébastien de La Forest Divonne
IHPE, Univ Montpellier, CNRS, Ifremer, Univ Perpignan Via Domitia, Montpellier, France

Juliette Pouzadoux
IHPE, Univ Montpellier, CNRS, Ifremer, Univ Perpignan Via Domitia, Montpellier, France

Océane Romatif
IHPE, Univ Montpellier, CNRS, Ifremer, Univ Perpignan Via Domitia, Montpellier, France

Caroline Montagnani
IHPE, Univ Montpellier, CNRS, Ifremer, Univ Perpignan Via Domitia, Montpellier, France

Guillaume Mitta
Ifremer, IRD, Institut Louis-Malardé, Univ Polynésie française, UMR 241 SECOPOL, Taravao, Tahiti - Polynésie française, France

Delphine Destoumieux-Garzon
IHPE, Univ Montpellier, CNRS, Ifremer, Univ Perpignan Via Domitia, Montpellier, France

Benjamin Gourbal
IHPE, Univ Montpellier, CNRS, Ifremer, Univ Perpignan Via Domitia, Perpignan, France
ORCID iD: 0000-0003-2097-2563

Guillaume M Charrière[#]
IHPE, Univ Montpellier, CNRS, Ifremer, Univ Perpignan Via Domitia, Montpellier, France
ORCID iD: 0000-0002-4796-1488

[#]EV and GC co-supervised the work.

Emmanuel Vignal[#]
IHPE, Univ Montpellier, CNRS, Ifremer, Univ Perpignan Via Domitia, Montpellier, France
ORCID iD: 0000-0002-2585-119X

For correspondence: emmanuel.vignal@umontpellier.fr
[#]EV and GC co-supervised the work.

Editors

Reviewing Editor
Bruno Lemaitre
École Polytechnique Fédérale de Lausanne, Lausanne, Switzerland

Senior Editor
Satyajit Rath
Indian Institute of Science Education and Research (IISER), Pune, India

Reviewer #1 (Public review):

Summary

In this manuscript, De La Forest Divonne et al. build a repertory of hemocytes from adult Pacific oysters combining scRNAseq data with cytologic and biochemical analyses. Three categories of hemocytes were described previously in this species (i.e. blast, hyalinocyte and granulocytes). Based on scRNAseq data, the authors identified 7 hemocyte clusters presenting distinct transcriptional signatures. Using Kegg pathway enrichment and RBGOA, the authors determined the main molecular features of the clusters. In parallel, using cytologic markers, the authors classified 7 populations of hemocytes (i.e. ML, H, BBL, ABL, SGC, BGC, and VC) presenting distinct sizes, nucleus sizes, acidophilic/basophilic, presence of pseudopods, cytoplasm/nucleus ratio and presence of granules. Then, the authors compared the phenotypic features with potential transcriptional signatures seen in the scRNAseq. The hemocytes were separated in a density gradient to enrich for specific subpopulations. The cell composition of each cell fraction was determined using cytologic markers and the cell fractions were analysed by quantitative PCR targeting major cluster markers (two per cluster). With this approach, the authors could assign cluster 7 to VC, cluster 2 to H, and cluster 3 to SGC. The other clusters did not show a clear association with this experimental approach. Using phagocytic assays, ROS, and copper monitoring, the authors showed that ML and SGC are phagocytic, ML produces ROS, and SGC and BGC accumulate copper. Then with the density gradient/qPCR approach, the authors identified the populations expressing anti-microbial peptides (ABL, BBL, and H). At last, the authors used Monocle to predict differentiation trajectories for each subgroup of hemocytes using cluster 4 as the progenitor subpopulation.

The manuscript provides a comprehensive characterisation of the diversity of circulating immune cells found in Pacific oysters.

Strengths

The combination of scRNAseq, cytologic markers and gradient based hemocyte sorting offers an integrative view of the immune cell diversity.
Hemocytes represent a very plastic cell population that has key roles in homeostatic and challenged conditions. Grasping the molecular features of these cells at the single-cell level will help understand their biology.

This type of study may help elucidate the diversification of immune cells in comparative studies and evolutionary immunology.

Weaknesses

Several figures show inconsistency leading to erroneous conclusions and some conclusions are poorly supported. Moreover, the manuscript remains highly descriptive with limited comparison with the available literature.

Comments on revisions:

The authors replied to most comments.

https://doi.org/10.7554/eLife.102622.3.sa1

Author response:

The following is the authors' response to the previous reviews

> ***Reviewer #1 (Recommendations for the authors):***
>
> *Major comments*
>
> *(1) Line 201: The threshold of 0.25 was maintained to select enriched genes, which minimize the value of the GO term enrichment analyses. It may notably explain why the term phagosome is enriched in cluster 7, while experimental data indicate that cluster 7 is not phagocytic. In addition, the authors mentioned in the 1st response to reviewer that they would include DotPlot to illustrate the specificity of the genes corresponding to the main GO terms. This should notably include the ribosomal genes found enriched in cluster 4, which constitute the basis used by the authors to call cluster 4 the progenitor cluster.*

We appreciate the reviewer's concern regarding our chosen log2FC threshold (0.25) for GO term enrichment. To assess the robustness of our approach, we tested more stringent thresholds (e.g., 0.5) and verified that our overall interpretations remain consistent. However, we acknowledge that certain GO terms, such as phagosome, may appear in clusters that are not primarily phagocytic. This is likely due to the fact that genes involved in vesicle trafficking, endo-lysosomal compartments and intracellular degradation processes overlap with those classically associated with phagocytosis.

Therefore, the KEGG-based enrichment of phagosome in cluster 7 does not necessarily imply active phagocytosis but could instead reflect these alternative vesicular processes. As we show, cluster 7 correspond to vesicular cells, and as seen in cytology we named these cells after their very high content of vesicular structures. As functional annotation based solely on transcriptomic data can sometimes lead to overinterpretations, we emphasize the importance of biological validation, which we have partially addressed through functional assays in this study.

Regarding the specificity of ribosomal gene expression in cluster 4, we analyzed the distribution of ribosomal genes expressed across all clusters, as shown in Supplementary Figure S1-J. This analysis demonstrates that cluster 4 is specifically enriched in ribosome-related genes, reinforcing its characterization as a transcriptionally active population. Given that ribosomal gene expression is a key feature often associated with proliferative or metabolically active cells, these findings support our initial interpretation that cluster 4 may represent an undifferentiated or progenitor-like population.

We acknowledge the reviewer's suggestion to include a DotPlot to further illustrate the specificity of these genes in cluster 4. However, we believe that Supplementary Figure S1-J already effectively demonstrates this enrichment by presenting the percentage of ribosomal genes per cluster. A DotPlot representation would primarily convey the same information in a different format, but without providing additional insight into the specificity of ribosomal gene expression within cluster 4.

> *(2) The lineage analysis is highly speculative and based on weak evidences. Initiating the hemocyte lineage to C4 is based on rRNA expression levels. C6 would constitute a better candidate, notably with the expression of PU-1, ELF2 and GATA3 that regulate progenitors differentiation in mammals (doi: 10.3389/fimmu.2019.00228, doi:10.1128/microbiolspec.mchd-0024-2, doi: 10.1098/rsob.180152) while C4 do not display any specific transcription factors (Figure 7I). In addition, the representation and interpretation of the transcriptome dynamics in the different lineages are erroneous. There are major inconsistencies between the data shown in the heatmaps Fig7C-H, Fig S10 and the dotplot in Fig7I. For example, Gata3 (G31054) and CgTFEB (G30997) illustrate the inconsistency. Fig S10C show GATA3 going down from cluster 4 to cluster 6 while Fig 7I show an increase level of expression in 6 compared to 4. CgTFEB (G30997) decrease from C4 to VC in Fig 7F while it increases according to Fig 7I. At last, Figure 7D: the umap show transition from C4 to C5 while the heatmap mention C4 to C6 (I believe there is a mix up with Figure 7E.*

We sincerely apologize for the inconsistencies noted between the different panels of Figure 7. These discrepancies resulted from using an incorrect matrix dataset during the initial representation. To address this issue, we have fully reprocessed the data and now provide a corrected and improved depiction of gene expression dynamics along the pseudotime trajectory. We are grateful to the reviewer for having help us to correct theses mistakes.

In the revised version, we offer a comprehensive and consistent representation of expression level variations for key genes identified by the Monocle3 algorithm. Supplementary Figure S10 now presents the average expression variation of these significant genes as a function of pseudotime. Based on this dataset, we carefully selected representative genes to construct panels C to H of Figure 7, ensuring coherence across all figures. These updated panels show both average expression levels and the percentage of expressing cells along the pseudotime trajectory, providing a clearer interpretation of transcriptomic dynamics.

We appreciate the reviewer's helpful feedback regarding our lineage analysis and the suggestion that cluster 6 might be a more appropriate progenitor based on the expression of mammalian-like transcription factors such as PU-1, ELF2, and GATA3. Below, we clarify our rationale for choosing cluster 4 as the root of the pseudotime and discuss the functional implications of the identified transcription factors.

We can hypothesize that clusters 4, 5, or 6 could each potentially represent early progenitor-like states, as these three clusters are transcriptionally close (Lines 539-541). These clusters have not yet been conclusively identified in terms of classical hemocyte morphology, and they appear to arise from ABL- or BBL-type cells. Our decision to root the pseudotime at cluster 4 was motivated by its strong expression of core transcription and translation genes, suggesting a particular stage of translation activity that was not observed for cluster 5 or cluster 6. Cluster 5 and 6 may correspond to a similar population of cells, most probably Blast-Like cells at different stages of cell cycle or differentiation engagement.

Although cluster 6 expresses PU-1, ELF2, and GATA3, which are known regulators of haematopoietic progenitor differentiation in vertebrates, it is essential to highlight that structural homology does not necessarily imply functional equivalence. Moreover, the expression of PU-1, ELF2, and GATA3 does not strictly characterize a population as

“undifferentiated” or progenitor-like. Studies such as those by Buenrostro et al. (Cell, 2018) have demonstrated that these transcription factors can remain active in or reemerge during more lineage-committed stages. For instance, PU-1 is essential for myeloid and B-cell differentiation, GATA3 is involved in T-lymphocyte lineage commitment (though transiently expressed in early progenitors), and ELF2 participates in lineage-specific pathways. Thus, their presence does not imply a primitive state but rather highlights their broader functional roles in guiding and refining lineage decisions. Functional annotation of these transcription factors in invertebrate systems remains speculative, particularly as morphological or molecular markers specific to these early hemocyte lineages are not yet fully established. Further functional assays (e.g., knockdown/overexpression or lineage tracing using cells (ABL and BBL) from clusters 4, 5 and 6) will be necessary to determine which hemocyte population harbor progenitor properties and differentiation potential.

To further address the reviewer’s concern, we performed complementary pseudotime analyses by initiating Monocle 3 trajectories from clusters 4, 5, and 6 individually, as well as collectively (4/5/6). These analyses (see attached figure) confirm that the overall differentiation topology remains unchanged regardless of the selected root, consistently revealing two main pathways: one leading to hyalinocytes and the other to the granular lineage (ML, SGC, and VC). This consistency strongly suggests that clusters 4, 5, and 6 represent related pools of progenitor-like cells. Therefore, choosing cluster 4 based on its transcription/translation readiness does not alter the inferred branching architecture of hemocyte differentiation.

We appreciate the reviewer’s suggestions, which have helped us improve our manuscript and clarify our rationale.

Author response image 1.

Representation of the trajectories obtained from Monocle3 analysis using different pseudotime origins, showing that changing the rooting did not alter the overall differentiation topology. (A) Pathways identified with cluster 4, (B) cluster 5, (C) cluster 6, and (D) cluster 4/5/6 origins.

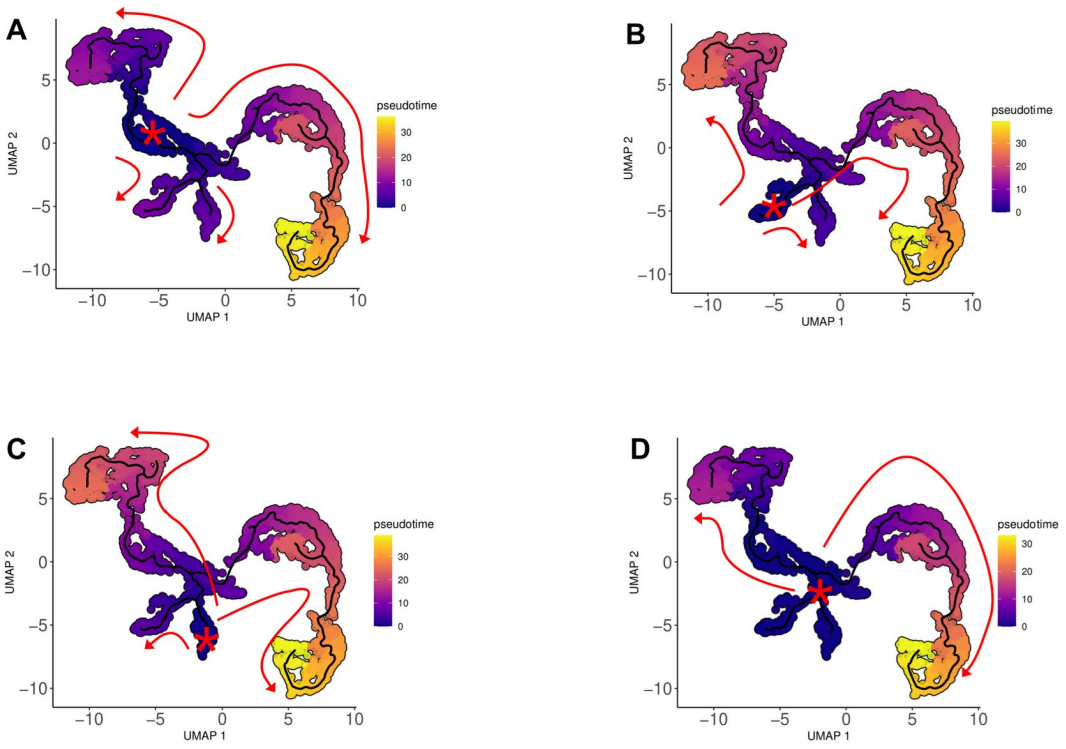

> *(3) Concerning the AMP expression analysis in Figure 6: the qPCR data show that Cg-BPI and Cg-Defh are expressed broadly in all fractions including 6 and 7, which is in conflict with the statement Line 473 indicating that SGC (fractions 6 and 7) is not expressing AMP. In addition, this analysis should be combined with the expression profile of all AMP in the scRNAseq data (list available in 10.1016/j.fsi.2015.02.040).*

We thank the reviewer for highlighting this point. We acknowledge that the qPCR data show expression of Cg-BPI and Cg-Defh across all fractions, including fractions 6 and 7 corresponding to SGC. However, our conclusion that SGCs do not express antimicrobial peptides (AMPs) was based on a correlation analysis rather than direct detection of AMPs in granular cells. Specifically, the qPCR experiments were designed to measure AMP expression levels in fractionated hemocyte populations relative to a control sample of whole hemolymph. We then performed a correlation analysis between AMP expression levels and the proportion of each hemocyte type in the fractions. This approach allowed us to infer a lower expression of AMP in granular cells, as reflected in the heatmap presented in Figure 6.

Regarding the suggestion to integrate AMP expression profiles from scRNA-seq data, we wrote that the limited sequencing depth of our scRNA-seq analysis was insufficient to accurately detect AMP expression (Ligne 472-473 → “However, due to the limited sequencing depth, the scRNA-seq analysis was not sensitive enough to reveal AMP expression.”. Additionally, many of the known AMPs of *Crassostrea gigas* are not annotated in the genome, further complicating their identification within the scRNA-seq dataset. As a result, we were unable to perform the requested integration of AMP expression profiles from scRNA-seq data.

> *(4) The transcription factor expression analysis is descriptive and the interpretation too partial. These data should be compared with other systems. Most transcription factors show functional conservation, notably in the inflammatory pathways, which can provide valuable information to understand the function of the clusters 5 and 6 for which limited data are available.*

We appreciate the reviewer's suggestion to compare the identified transcription factors with other systems. However, since we did not perform a detailed phylogenetic analysis of the transcription factors identified in our dataset, we refrain from making assumptions about their functional conservation across species. Our analysis aims to provide a descriptive overview of transcription factor expression patterns in hemocyte clusters, which serves as a foundation for future functional studies. While transcription factor profiles may provide insights into the potential roles of clusters 5 and 6, assigning precise functions based solely on bioinformatic predictions remains speculative. Further experimental validation, including functional assays and evolutionary analyses, would be necessary to confirm the roles of these transcription factors, which is beyond the scope of the present study.

> *Minor comments*
>
> *Line 212-213: the text should be reformulated. In the result part, it is more important to mention that the reannotation is based on conserved proteins functions than to mention the tool Orson.*

We have reworded this section to emphasize that the updated annotation is *function-based*, using Orson primarily as the *bioinformatics tool* for improved GO annotation. We now place the emphasis on the conserved protein functions underlying the reannotation. Lines 212-215 : "Using the Orson pipeline (see Materials and Methods), these files were used to extract and process the longest CDSs for GO-term annotation, and we then reannotated each predicted protein by sequence homology, assigning putative functions and improving downstream GO-term analyses."

> *Figure 2: I would recommend homogenizing the two Dotplot representation with the same color gradient and representing the gene numbers in both case.*

We appreciate the reviewer's suggestion to improve the clarity and consistency of Figure 2. In response, we have homogenized the color gradients across the two DotPlot representations and have included gene numbers in both cases to ensure a more uniform and informative visualization.

> *Table 2: pct1 and pct2 should be presented individually like in table 1*

We now present these columns separately (pct1, pct2) as in Table 1, so readers can compare the fraction of expressing cells in each cluster more transparently.

> *Line 403-414: how many cells were quantified for the phagocytic experiments ?*

We have added the exact number of cells that were counted to determine phagocytic indices and the number of technical/biological replicates. Line 411, the text was modified : "Macrophage-like cells and small granule cells showed a phagocytic activity of 49 % and 55 %, respectively, and a phagocytosis index of 3.5 and 5.2 particles per cell respectively (Fig. 5B and Supp. Fig. 7B), as confirmed in 3 independent experiments examining a total of 2,807 cells."

> *Line 458: for copper staining, how many cells and how many replicates were done for the quantification ?*

We have specified the number of hemocytes and number of independent replicates used when quantifying rhodanine-stained (copper-accumulating) cells. Line 458 the following text was added : "and a total of 1,562 cells were examined across three independent experiments."

> *Line 461: what are the authors referring to when mentioning the link between copper homeostasis and scRNAseq?*

Single-cell RNA sequencing (scRNA-seq) analysis revealed an upregulation of several copper transport– related genes, including G4790 (a copper transporter) with a 2.7 log2FC and a pct ratio of 42, as well as the divalent cation transporters G5864 (zinc transporter ZIP10) and G4920 (zinc transporter 8), specifically in cluster 3 cells identified as small granule cells. These findings reinforce a potential role for this cluster in metal homeostasis.

We modified lines 462-467 as : " These results provide functional evidence that small granule cells (SGCs) are specialized in metal homeostasis in addition to phagocytosis, as suggested by the scRNA-seq data identifying cluster 3. Specifically, single-cell RNA sequencing revealed an upregulation of copper transport– related genes, including G4790 (a copper transporter) with a 2.7 log2FC and a pct ratio of 42, reinforcing the role of SGCs in copper homeostasis (see Supp. File S1)."

> *Line 611: it would be nice to display the enrichment of the phagocytic receptor in cluster 3 (dotplot or feature plot) to illustrate the comment.*

We appreciate the reviewer's insightful suggestion regarding a more comprehensive analysis of phagocytic receptors. While a full inventory is beyond the scope of this study, we acknowledge the value of such an approach and hope that our findings will serve as a foundation for future investigations in this direction.

Although we have highlighted certain phagocytic receptors (e.g., a scavenger receptor domain-containing gene) in our scRNA-seq dataset, it is beyond the scope of the current study to inventory all phagocytosisrelated receptors in the *C. gigas* genome, which itself would be a substantial undertaking. Moreover, singlecell RNA sequencing captures only about 15–20% of each cell's mRNA, so we inherently lose a significant portion of the transcriptome, further limiting our ability to pinpoint all relevant phagocytic receptor genes. Adding more figures to cover every candidate receptor would risk overloading this paper, thus we focus on the most prominent examples. A promising approach for more exhaustive analysis would involve efficiently isolating granulocytes (e.g., via Percoll gradient) and performing targeted RNA-seq on this cell population to thoroughly explore genes involved in phagocytosis.

> *Line 640-644: the authors mentioned that ML may be able to perform ETosis based on the oxidative burst.*
>
> *This hypothesis requires further evidences. Are other markers of ETosis expressed in this cell type?*

We agree that additional experimental evidence (e.g., detection of histone citrullination, extracellular DNA networks) is necessary to confirm ETosis in molluscan immune cells. We present ML-mediated ETosis only as a speculative possibility based on oxidative burst capacity as it was shown in different pieces of work that ETosis is inhibited by NADPH inhibitors (Poirier et al. 2014). Nevertheless, the expression of histones in the macrophage-like cluster (cluster 1) reinforces this possibility, as histone modifications play a key role in chromatin decondensation during ETosis.

> ***Reviewer #2 (Recommendations for the authors):***
>
> *Figure 1: In Figure 1B, the cell clusters are named 1 to 7, whereas in Figure 1C they are displayed as clusters 0 to 6. There is a mismatch between the identification of the clusters.*

We thank the reviewer for identifying this inconsistency. The cluster numbering has been corrected to ensure consistency between Figures 1B and 1C.

> *Figure 2B: the font size could be increased for greater clarity.*

We thank the reviewer for this suggestion. The font size in Figure 2B has been increased to improve clarity and readability.

> *Line 221: "Figures 2B, C and D" appears to refer to Figure S2 rather than the main Figure 2.*

The text has been corrected to properly reference the figure.

> *Line 754: "Anopheles gambiae" should be italicised*

We thank the reviewer for pointing this out. "*Anopheles gambiae*" has been italicized accordingly.

Bibliography

Integrated Single-Cell Analysis Maps the Continuous Regulatory Landscape of Human Hematopoietic

Differentiation. Buenrostro, Jason D. et al. Cell, Volume 173, Issue 6, 1535 - 1548.e16

Antimicrobial Histones and DNA Traps in Invertebrate Immunity

Poirier, Aurore C. et al. Journal of Biological Chemistry, Volume 289, Issue 36, 24821 - 24831

https://doi.org/10.7554/eLife.102622.3.sa0